

A theory of intense-field dynamic alignment and high harmonic generation from coherently rotating molecules and interpretation of intense-field ultrafast pump-probe experiments

A. Abdurrouf^{1,2*} and F.H.M. Faisal^{1†}

¹*Fakultät für Physik, Universität Bielefeld, Postfach 100131, D-33501 Bielefeld, Germany and*

²*Department of Physics, University of Brawijaya, Malang, Indonesia 65145*

A theory of ultra-fast pump-probe experiments proposed by us earlier [F.H.M. Faisal *et al.*, Phys. Rev. Lett. **98**, 143001 (2007) and F.H.M. Faisal and A. Abdurrouf, Phys. Rev. Lett. **100**, 123005 (2008)] is developed here fully and applied to investigate the phenomena of dynamic alignment and high harmonic generation (HHG) from coherently rotating linear molecules. The theory provides essentially analytical results for the signals that allow us to investigate the simultaneous dependence of the HHG signals on the two externally available control parameters, namely, the relative angle between the polarizations, and the delay-time between the two pulses. It is applied to investigate the characteristics of high harmonic emission from nitrogen and oxygen molecules that have been observed experimentally in a number of laboratories. The results obtained both in the time-domain and in the frequency-domain are compared with the observed characteristics as well as directly with the data and are found to agree remarkably well. In addition we have predicted the existence of a “magic” polarization angle at which all modulations of the harmonic emission from nitrogen molecule changes to a steady emission at the harmonic frequency. Among other things we have also shown a correlation between the existence of the “magic” or critical polarization angles and the symmetry of the active molecular orbitals, that is deemed to be useful in connection with the “inverse problem” of molecular imaging from the HHG data.

PACS numbers: 32.80.Rm, 32.80.Fb, 34.50.Rk, 42.50.Hz

I. INTRODUCTION

In recent years there has been much interest and progress in understanding the interaction of atoms and molecules with intense laser fields (e.g. reviews [1, 2]). Among the phenomena observed, the high-order harmonic generation (HHG) is of particular interest, no less because of its potential applications as a source of coherent ultraviolet light and/or for generation of ultrashort attosecond laser pulses. In contrast to atoms, molecules have extra degrees of freedom such as vibration, and rotation of the molecular frame, and have additional symmetry properties, that give rise to richer physical phenomena when they interact with intense laser pulses. Among them is the phenomenon of alignment of linear molecules by strong and long laser pulses which has been investigated in the past [3, 4, 5, 6]. Much interest has recently been generated by the observation of recurrent dynamic alignments of linear molecules like N₂ and O₂ [7, 8], interacting with intense ultrashort laser pulses. They are monitored, for example, by non-destructive high harmonic generation signals from intense-field pump-probe experiments with delayed pairs of intense ultrashort pulses [9, 10, 11, 12, 13]. The dynamic HHG signals have been used also to “reconstruct” the molecular orbitals [14, 15, 16], to investigate proton motions [17] and molecular dynamics [18].

In this paper we derive fully a recently proposed [19, 20] quantum theory of intense-field dynamic alignment and high harmonic generation from linear molecules and apply it to analyze the observed dynamical HHG signals for N₂ and O₂ molecules. Theoretical expressions for the signals are given analytically as a simultaneous function of the two external operational parameters – the delay time, t_d , and the relative polarization angle, α , between the pump and the probe pulse [9, 10, 11, 12, 13].

Before proceeding further, we briefly discuss the main experimental characteristics of dynamic alignment and the HHG signals as observed for N₂ and O₂. We recall at the out set that the quantum measure of dynamical alignment of a rotating molecule is the quantum expectation value (with respect to the rotational wave-packet states induced by the pump pulse) of the “alignment operator” $\cos^2 \theta$, that is averaged over the Boltzmann distribution of the initially occupied rotational states: $A(t_d) \equiv \langle \langle \cos^2 \theta \rangle \rangle(t_d)$, where θ is the angle between the molecular axis and the probe polarization direction; the double angular brackets stand for the expectation value with respect to the rotational wave-packets (inner brackets) and the statistical average with respect to the Boltzmann distribution (outer brackets) of the initially occupied rotational states. It was observed experimentally [9, 10, 11, 12, 13] that the dynamic (or delay-time dependent) HHG signal for N₂ mimicked the “alignment measure” $A(t_d)$. It exhibited the phenomenon of rotational revivals [3, 6, 21] including the “full-revival” with a period $T_r = \frac{1}{2Bc}$, where B is the rotational constant [22], as well as a $\frac{1}{2}$ -revival, and a $\frac{1}{4}$ -revival. They are consistent with the time dependence of $A(t_d)$ defined

*Electronic address: a.abdurrouf@googlemail.com

†Electronic address: ffaisal@physik.uni-bielefeld.de

above, since the operator $\cos^2\theta$ can couple the rotational states with $\Delta J = \pm 2$ (Raman allowed transitions) among the rotational states of the induced wavepackets, and thus can give rise to fractional revival periods associated with the corresponding beat frequencies. In the case of O_2 , unexpectedly, an additional $\frac{1}{8}$ -revival appeared in the HHG signal [11, 12, 13]. The latter is impossible for the alignment measure $A(t_d)$ to account for, since it can not couple the rotational states with $\Delta J = \pm 4$, that could give rise to a beat period $\frac{1}{8}T_r$. Thus, to fit their data of O_2 , Itatani *et al.* [11] proposed, empirically, to consider the expectation value of the operator $B(t_d) \equiv \langle\langle \sin^2 2\theta \rangle\rangle(t_d)$. Subsequently, some of the early theoretical models of the HHG signal (e.g. [23, 24, 25]) gave a similar result for O_2 and thus appeared to justify the empirical fit. Such a model also suggests that the maximum HHG signal for N_2 can occur when the field polarization and the molecular axis were parallel, whereas the maximum signal of O_2 would occur when they are “diagonal” (i.e. make an angle $\theta = 45^\circ$). Unlike the time dependent signals themselves, their Fourier transform (*F.T.*), with sharply defined individual spectral lines and series, provide an alternative (and rather more precise) means of studying the dynamic alignment phenomenon. More recent experimental observations of the dynamic HHG signals for N_2 and O_2 , and their *F.T.* have revealed surprising characteristics that can not be fully understood in terms of the earlier considerations. Thus:

(a) Kanai *et al.* [12] found that their experimental HHG signals for N_2 and O_2 could not be well fitted, respectively, by the expectation values of the operators $\cos^2\theta$ and $\sin^2 2\theta$, alone. They considered empirically additional operators involving *higher* powers of $\cos^2\theta$, or Legendre polynomials, to fit their data.

(b) Miyazaki *et al.* [13] measured the dynamical HHG signals of N_2 and O_2 and Fourier transformed their signals and found not only spectral series containing strong Raman allowed but also weak Raman forbidden and anomalous lines, for both N_2 and O_2 .

(c) Itatani *et al.* [14] observed that the HHG signal from dynamically aligned N_2 was enhanced when the pump polarization was taken parallel to the probe polarization, and were suppressed when the polarizations were taken to be perpendicular.

(d) Kanai *et al.* [12] and Miyazaki *et al.* [13, 26] measured the HHG signal for the diatomic N_2 , O_2 , and the triatomic CO_2 , for different relative angles α between the pump and probe polarizations, and observed that the HHG signal modulations are not only smaller in the perpendicular case, compared to the parallel case, but also are of *opposite phase* in the two geometries.

(e) Kanai *et al.* [12] proposed a planar emission model of HHG which produced an opposite phase relation, as observed, but it did not yield the *unequal* modulation amplitudes, observed in the two geometries.

(f) The present theory predicted (cf. [20] and below) a “magic” polarization angle, $\alpha_c \approx 55^\circ$, at which the har-

monic emission from coherently rotating molecules with σ_g orbital symmetry (e.g. N_2) becomes equal for *all* delay times t_d . Most recent observations by Yoshii *et al.* [27, 55] appear to confirm the same.

In this paper we present an *ab initio* development of the above mentioned theory [19, 20] that is shown to provide a unified theoretical account of all the phenomena noted above and other related characteristics of dynamic alignments and the HHG signals from the aligning molecules, as well as their Fourier spectra, that have been observed experimentally. To this end, below we begin with a short schematic description of a typical intense-field pump-probe experiment on dynamic alignments and the molecular HHG signals as a function of (a) the time delay, t_d , and (b) the relative polarization angle, α , between the pump and the probe pulse. In Sec. II, III and IV, we systematically derive the S-matrix theory of molecular alignment and dynamic HHG signal from an ensemble of freely rotating linear molecule, discuss the connection between the “one” - and the “many”-molecule signals, and the relation between the quantum amplitude for the emission of the HHG photons and the expectation value of the dipole transition moment. In Sec. V, we apply the theory to N_2 and O_2 molecules and obtain analytic expressions for the “HHG operators” and the HHG *signals* for an arbitrary, α , and delay times, t_d . In Sec. VI. we use the theoretical expressions to explicitly calculate the HHG signals for specific experimental parameters, for the linear molecules N_2 and O_2 , both in the time domain and in the frequency domain, and discuss the results with reference to the corresponding experimental observations. In addition, we investigate in section VII a number of related problems of general interest including the influence of the probe pulse on the dynamic alignment, the effect of the initial temperature on the HHG signal, and the *mean energy* of the molecule after interaction with the pump pulse. We also discuss two other definitions used earlier for the HHG signal, as well as investigate the case of “adiabatic alignment” of a linear molecule, within the present theory, in the limit of long pulse durations. We end with a concluding summary in Sec. VIII.

In Fig. 1 we show a schematic of a typical intense-field pump-probe experiment. A laser beam is first split into two parts, L_1 and L_2 , by a beam splitter (*BS*) with a desired ratio of the beam intensities. The probe-pulse L_2 is delayed by passing through a delay line system (*D*), by a finite amount t_d , with respect to the pump-pulse L_1 and both are sent through a beam mixer (*BM*) to the target gas molecules from a gas jet. The high harmonic signal produced by the probe pulse is recorded by the detector system for each selected values of t_d . In addition, a polarizer *P* can be inserted to rotate the angle of polarization of the probe pulse with respect to the polarization direction of the pump pulse at any desired angle α . The pulses are generally assumed to be effectively non-overlapping ($t_d \neq 0$) and that they are shorter than the period of the rotational degrees of freedom of interest.

Note that both t_d and α provide controllable parameters

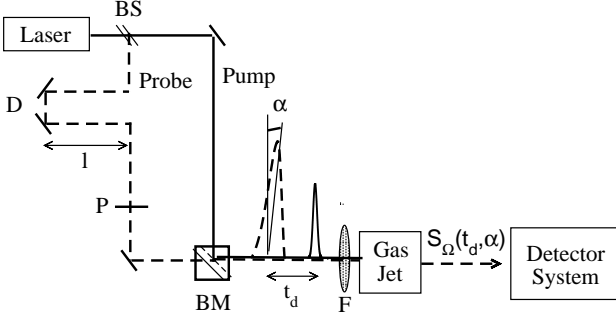


Figure 1: A scheme of a typical pump-probe experiment. See text for further explanation.

II. A QUANTUM THEORY OF INTENSE-FIELD PUMP-PROBE EXPERIMENTS AND MOLECULAR HIGH HARMONIC GENERATION SIGNALS

A. Total Hamiltonian and Equations of Motions of the Dynamical System

Within the adiabatic Born-Oppenheimer approximation of the target molecule, the total Hamiltonian of the system can be written [19]: (in a.u.: $e = \hbar = m = \alpha c = 1$) as,

$$H_{tot}(t) = H_N + V_{N-L_1}(t) + H_e + V_{e-L_2}(t - t_d) \quad (1)$$

where H_N is the nuclear Hamiltonian, $V_{N-L_1}(t)$ is the interaction due to the pump pulse with the nuclear motion at time t , H_e is the electronic Hamiltonian, and $V_{e-L_2}(t - t_d)$ is the interaction of the probe pulse with the active electron at a delay t_d . We describe the two laser pulses (in the long-wavelength dipole-approximation) of the laser fields, $F(\phi_j(t)) \equiv f(t) \cos(\phi_j(t))$ and the corresponding the vector potentials by $A(\phi_j(t)) = -\frac{c}{\omega} f(t) \sin(\phi_j(t))$, where $f(t)$ is the slowly varying envelope of the electric field (compared to the period of the high harmonics, or the electron motion). The phase $\phi_j(t)$ of the field at the position of the active electron of the molecule is given by $\phi_j(t) = (\omega t - \mathbf{k}_\omega \cdot \mathbf{X}_j)$, where the *C.M.* of the molecule is assumed to be located at a position “ \mathbf{X}_j ”; ω and \mathbf{k}_ω are the laser of frequency and the wavenumber, respectively. For the sake of simplicity of writing, we may suppress the notation the full \mathbf{X}_j and t dependence of the phase factor $\phi_j(t)$ unless otherwise needed explicitly, e.g. while summing coherently the “many-molecule” emission amplitudes from different locations $\{\mathbf{X}_j\}$ to obtain the total amplitude associated with the signal macroscopically coherent signal. It will be found that the coherent signal appears significantly for the “elastic” scattering (the final state of the molecule

is the same as the initial state) with respect to the target molecule, and (for an ideal gas medium) along the forward direction of the incident field (cf. [2, §4], and references cited in that section).

Thus, we may write the laser-molecule interaction Hamiltonians appearing above as given by

$$V_{N-L_1}(t) = -\boldsymbol{\mu} \cdot \mathbf{F}_1(t) - \frac{1}{2} \mathbf{F}_1(\phi_j(t)) : \boldsymbol{\alpha} : \mathbf{F}_1(\phi_j(t)) \quad (2)$$

where $\boldsymbol{\mu}$ is the permanent dipole moment (if non-zero) and $\boldsymbol{\alpha}$ with Cartesian components $\alpha_{ii'}$; $(i, i') = (1, 2, 3)$ is the polarizability *tensor* of the molecule (always non-zero); and

$$V_{e-L_2}(\phi_j(t - t_d)) = -\hat{\mathbf{d}}_e \cdot \mathbf{F}(\phi_j(t - t_d)) \quad (3)$$

where $\hat{\mathbf{d}}_e$ stands for the electronic dipole *operator*.

B. Total Wavefunction in Intense-field S-Matrix Theory

We first consider a systematic solution of the time-dependent Schrödinger equation of the system

$$i \frac{\partial}{\partial t} \Psi(t) = H_{tot}(t) \Psi(t) \quad (4)$$

using the general technique of intense-field many-body S-matrix theory (IMST) [2]. In this approach the total wavefunction of the system satisfying a given initial (final) condition can be written as a series expansion in such a way that the dominant virtual states, when present, can appear already in the leading terms of the series. To this end we introduce three partitions of the same total Hamiltonian, referring to the initial, “*i*”, the final, “*f*”, and the (deemed to be relevant) intermediate virtual state, “*0*”, interactions plus the corresponding “reference” Hamiltonians:

$$\begin{aligned} H_{tot}(t) &= H_i + V_i(t) \\ &= H_f(t) + V_f(t) \\ &= H_0(t) + V_0(t). \end{aligned} \quad (5)$$

It is also useful to define the reference Green’s functions associated with the reference Hamiltonians, $H_s(t)$; $s \equiv i, f, 0$:

$$\left(i \frac{\partial}{\partial t} - H_s(t) \right) G_s(t, t') = \delta(t - t'). \quad (6)$$

In general, the Green functions can be obtained from the complete set of the fundamental solutions, $|\psi_j^{(s)}(t)\rangle$ of the Schrödinger equations governed by the reference Hamiltonians $H_s(t)$; $s = i, f, 0$:

$$G_s(t, t') = -i \theta(t - t') \sum_{all j} |\psi_j^{(s)}(t)\rangle \langle \psi_j^{(s)}(t')| \quad (7)$$

The validity of the solutions Eq. (6) can be readily established by operating on the left hand side of Eq. (7) with $(i\frac{\partial}{\partial t} - H_0(t))$, using Eq. (6) and the completeness of the fundamental solutions, $\sum_j |\psi_j^{(s)}(t)\rangle \langle \psi_j^{(s)}(t)| = \mathbf{1}$ and the relation $\frac{\partial}{\partial t} \theta(t-t') = \delta(t-t')$, to obtain a delta-function integration on the right hand side, followed by the obvious simplification. Thus, we can express the total wavefunction of the interacting system, evolving from an arbitrary initial state, $|\chi_i(t)\rangle$, as a series:

$$|\Psi(t)\rangle = \sum_{j=0}^{\infty} |\Psi_i^{(j)}(t)\rangle \quad (8)$$

with

$$|\Psi_i^{(0)}(t)\rangle = |\chi_i(t)\rangle \quad (9)$$

$$|\Psi_i^{(1)}(t)\rangle = \int_{t_i}^{t_f} dt_1 G_f^0(t, t_1) V_i(t_1) |\chi_i(t_1)\rangle \quad (10)$$

$$\begin{aligned} |\Psi_i^{(2)}(t)\rangle &= \int_{t_i}^{t_f} \int_{t_i}^{t_f} dt_2 dt_1 G_f^0(t, t_2) V_f(t_2) G_0(t_2, t_1) \\ &\quad \times V_i(t_1) |\chi_i(t_1)\rangle \\ &\dots\dots \end{aligned} \quad (11)$$

and

$$\begin{aligned} |\Psi_i^{(n)}(t)\rangle &= \int_{t_i}^{t_f} \dots\dots \int_{t_i}^{t_f} \int_{t_i}^{t_f} dt_n \dots\dots dt_2 dt_1 G_f^0(t, t_n) \\ &\quad \times V_f(t_n) \dots\dots G_0(t_3, t_2) V_f(t_2) G_0(t_2, t_1) \\ &\quad \times V_i(t_1) |\chi_i(t_1)\rangle. \end{aligned} \quad (12)$$

III. MANY-MOLECULE VS. ONE-MOLECULE SIGNALS

A. Transition Amplitudes for High Harmonic Generation

Emission of a harmonic photon of frequency $\Omega = n\omega$ and wavevector \mathbf{K}_Ω , from its vacuum state $|0_\Omega\rangle$ (zero occupation number in Fock-space), into a singly occupied number state, $|1_\Omega\rangle$, is fundamentally a quantum electrodynamical process i.e. due to the interaction of the active electron with the vacuum-field albeit in the presence of the intense external laser field. Its theoretical formulation therefore clearly requires one to consider at least the combined state of the interacting “laser field (semiclassical) + molecule + vacuum-field”- system in the extended space consisting of the direct product of the ordinary space of “laser field (semiclassical) + molecule” and the occupation number space of the vacuum and the emitted photon (cf. e.g. [2, §4.5]). Nevertheless, exactly the

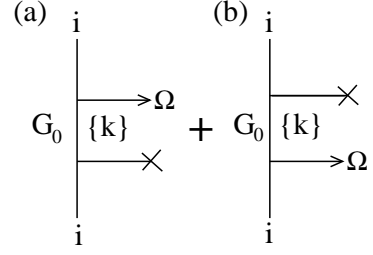


Figure 2: Quantum amplitude for coherent emission of a high harmonic photon (frequency Ω) is the sum of a direct (a) and a time-reversed (b) diagram.

same result for the single photon HHG emission amplitude can also be obtained using the ordinary quantum mechanics, simply by taking the quantum electrodynamically normalized interaction $V^*(t)$ for the spontaneous emission of a photon of frequency Ω and wavevector \mathbf{K}_Ω (cf. [28, 29, Lecture 2]):

$$V^*(t) = N_\Omega e^{i\Phi_j(t)} \boldsymbol{\epsilon}_\Omega \cdot \hat{\mathbf{d}}_e \quad (13)$$

In the above, $N_\Omega \equiv \sqrt{\frac{2\pi\hbar\Omega}{L^3}}$, L^3 is the quantization volume, $\boldsymbol{\epsilon}_\Omega$ is the polarization vector of the emitted photon, and $\hat{\mathbf{d}}_e$ is the usual electronic transition dipole operator; the phase $\Phi_j(t) = (\Omega t - \mathbf{k}_\omega \cdot \mathbf{X}_j)$. As usual in the present dipole approximation, we have neglected the retardation factor, $e^{-i\mathbf{K}_\Omega \cdot \mathbf{r}} \approx 1$; we may note explicitly that the exact position of the electron with respect to an arbitrary coordinate origin is given by $\mathbf{X}_j + \mathbf{r}$, where as before \mathbf{X}_j is the C.M. of the j th molecule and \mathbf{r} is the position of the electron with respect to the C.M. of the molecule.

The HHG amplitude for the emission of a harmonic frequency Ω from the j th molecule is given by (cf. [2, §4]) by the sum of two “Feynman-like” diagrams, (a) and (b), shown in Fig. 2. The diagram (a) corresponds to the so-called “direct” amplitude (associated with the retarded Green’s function), whereas the diagram (b) corresponds with the “time-reversed” amplitude (associated with the advanced Green’s function). The amplitude for the harmonic emission process can be written down analytically from diagram (a) by reading in the forward (upward) direction of time: First, the molecule is prepared by the “pump” laser pulse in the state $i \equiv |\Phi_i(t)\rangle$. Next, the molecule interacts with the probe laser field (short horizontal line with a cross), then it propagates through $G_0 = G_0^{(+)}$ (vertical line). Next it interacts with the vacuum-field by $V^{(*)}$ (horizontal line ending in Ω), and emits the harmonic photon of frequency Ω , and finally returns to the *same* state $i \equiv |\Phi_i(t)\rangle$ as before. A similar interpretation holds for the time reversed diagram (b) except that here the system evolves backward in time thorough $G_0 = G^{(-)}$. The quantum amplitude $A_j(\Omega)$, for the emission of the HHG photon of frequency Ω , and wavenumber \mathbf{K}_Ω , from the molecule located at

\mathbf{X}_j , is given by the *sum* of the two diagrams:

$$A_j(\Omega) = \text{diag.}(a) + \text{diag.}(b) \quad (14)$$

Mathematically, we have

$$\begin{aligned} \text{diag.}(a) &= -i \int_{-\infty}^{\infty} dt \int_{-\infty}^{\infty} dt' \langle \phi_i(t) | V^*(t) \\ &\quad \times G_0^{(+)}(t, t') V_{e-L_2}(t' - t_d) | \chi_i(t') \rangle \end{aligned} \quad (15)$$

and,

$$\begin{aligned} \text{diag.}(b) &= -i \int_{-\infty}^{\infty} dt \int_{-\infty}^{\infty} dt' \langle \phi_i(t') | V_{e-L_2}(t' - t_d) \\ &\quad \times G_0^{(-)}(t', t) V^*(t) | \chi_i(t) \rangle \end{aligned} \quad (16)$$

B. A Relation between HHG Amplitude and *F.T.* of Dipole Expectation Value

1. Recasting the quantum HHG amplitude

Before proceeding further, we consider the relation between the quantum HHG amplitude, Eq. (14), and the expectation value of the electric dipole operator, $\hat{\mathbf{d}}_e$, that is popularly used for calculations of HHG signals. To this end we first rewrite the quantum amplitude Eq. (15) by introducing the first order wavefunction $\Psi^{(1)}$ (cf. Eq. (10)) that arises from the initial state $|\chi_i(t)\rangle$ due to the interaction with the probe pulse:

$$\begin{aligned} |\Psi^{(1)}(t)\rangle &= \int_{-\infty}^{\infty} dt' G_0^{(+)}(t, t') \\ &\quad \times V_{e-L_2}(t' - t_d) | \chi_i(t') \rangle \end{aligned} \quad (17)$$

We may first rewrite Eq. (15) as:

$$\begin{aligned} \text{diag.}(a) &= -i \int_{-\infty}^{\infty} dt \langle \chi_i(t) | V^*(t) | \Psi^{(1)}(t) \rangle \\ &= -i \int_{-\infty}^{\infty} dt e^{i(\Omega t - \mathbf{K}_\Omega \cdot \mathbf{X}_j)} \\ &\quad \times \langle \chi_i(t) | N_\Omega \epsilon_\Omega \cdot \hat{\mathbf{d}}_e | \Psi^{(1)}(t) \rangle \end{aligned} \quad (18)$$

where we have used the explicit form of the interaction $V^*(t)$. Next we rewrite Eq. (16) using a standard relation satisfied by the advanced and the retarded Green functions (e.g. [29]):

$$G_0^{(-)}(t', t) = [G_0^{(+)}(t, t')]^* \quad (19)$$

We also note that the laser-molecule interaction is real (Hermitian), i.e.

$$V_{e-L_2}(t) = [V_{e-L_2}(t)]^* \quad (20)$$

Thus, the integral over dt' in Eq. (16) can be rewritten as,

$$\begin{aligned} \text{diag.}(b) &= -i \int_{-\infty}^{\infty} dt \int_{-\infty}^{\infty} dt' \langle \chi_i(t') | V_{e-L_2}(t' - t_d) \\ &\quad \times G_0^{(-)}(t', t) V^*(t) | \chi_i(t) \rangle \\ &= -i \int_{-\infty}^{\infty} dt \int_{-\infty}^{\infty} dt' \\ &\quad \times [G_0^{(+)}(t, t') V_{e-L_2}(t' - t_d) | \chi_i(t') \rangle]^* \\ &\quad \times V^*(t) | \chi_i(t) \rangle \\ &= -i \int_{-\infty}^{\infty} dt \langle \Psi^{(1)}(t) | V^*(t) | \chi_i(t) \rangle \\ &= \int_{-\infty}^{\infty} dt e^{i(\Omega t - \mathbf{K}_\Omega \cdot \mathbf{X}_j)} \\ &\quad \times \langle \Psi^{(1)}(t) | N_\Omega \epsilon_\Omega \cdot \hat{\mathbf{d}}_e | \chi_i(t) \rangle \end{aligned} \quad (21)$$

Hence, adding Eqs. (18) and (21), we get the quantum HHG amplitude in the suggestive form:

$$\begin{aligned} A_j(\Omega) &= -i N_\Omega \epsilon_\Omega \cdot \int_{-\infty}^{\infty} dt e^{i(\Omega t - \mathbf{K}_\Omega \cdot \mathbf{X}_j)} \\ &\quad \times \left\{ \langle \chi_i(t) | \hat{\mathbf{d}}_e | \Psi^{(1)}(t) \rangle + \langle \Psi^{(1)}(t) | \hat{\mathbf{d}}_e | \chi_i(t) \rangle \right\} \\ &= -i N_\Omega \epsilon_\Omega \cdot \int_{-\infty}^{\infty} dt e^{i(\Omega t - \mathbf{K}_\Omega \cdot \mathbf{X}_j)} \\ &\quad \times \left\{ \langle \chi_i(t) | \hat{\mathbf{d}}_e | \Psi^{(1)}(t) \rangle + c.c. \right\} \end{aligned} \quad (22)$$

where “c.c.” stands for the complex conjugate.

2. Dipole expectation value

The expectation value of the dipole operator, $\mathbf{D}_{i,i}(t)$, of the transition dipole operator can be calculated within the lowest order KFR approximation [30, 31, 32] of the wavefunction of the system as follows:

$$\begin{aligned} \mathbf{D}_{i,i}(t) &= \langle \Psi(t) | \hat{\mathbf{d}}_e | \Psi(t) \rangle \\ &= \langle \chi_i(t) | \hat{\mathbf{d}}_e | \chi_i(t) \rangle \\ &\quad + \left\{ \langle \chi_i(t) | \hat{\mathbf{d}}_e | \Psi^{(1)}(t) \rangle \right. \\ &\quad \left. + \langle \Psi^{(1)}(t) | \hat{\mathbf{d}}_e | \chi_i(t) \rangle \right\} + \dots \\ &= \left\{ \langle \chi_i(t) | \hat{\mathbf{d}}_e | \Psi^{(1)}(t) \rangle + c.c. \right\} + \dots \end{aligned} \quad (23)$$

Note that the zeroth order term in the first line above vanishes for centrosymmetric systems; we have also neglected the quadratic powers of the first order KFR-correction (and the higher order terms).

Combining Eq. (23) with Eq. (22), the quantum HHG amplitude can be expressed in the form

$$A_j(\Omega) = -i e^{-i \mathbf{K}_\Omega \cdot \mathbf{X}_j} N_\Omega \epsilon_\Omega \cdot \int_{-\infty}^{\infty} dt e^{i \Omega t} \mathbf{D}_{i,i}(t) \quad (24)$$

Thus, the quantum HHG amplitude is clearly *proportional* to the Fourier transform (*F.T.*) of the expectation value of the transition dipole operator, Eq. (23). We may recall that the proportionality constant N_Ω above is of quantum electrodynamical origin and can *not* be derived from the classical electrodynamics alone [33].

In practice, the *F.T.* of interest can be conveniently obtained by Fast Fourier transform (or *FFT*) numerically [34]. Alternatively, for “slowly varying” pulse envelopes (compared to the high harmonic frequency) one may express the *F.T.* of $\mathbf{D}_{i,i}(t)$ as a Fourier series [35]:

$$\mathbf{D}_{i,i}(t) = \sum_n e^{-in(\omega t - \mathbf{k}_\omega \cdot \mathbf{X}_j)} \tilde{\mathbf{D}}(n\omega) \quad (25)$$

where $\tilde{\mathbf{D}}(n\omega)$ is the *F.T.* evaluated at the n th harmonic frequency $\Omega = n\omega$. Thus, in terms of the *F.T.* components, the HHG amplitude $A_j(\Omega)$ becomes,

$$A_j(\Omega) = \sum_n -2\pi i \delta(\Omega - n\omega) e^{-i(\mathbf{K}_\Omega - n\mathbf{k}_\omega) \cdot \mathbf{X}_j} \times N_\Omega \epsilon_\Omega \cdot \tilde{\mathbf{D}}_{i,i}(n\omega) \quad (26)$$

where we have carried out the time integration over dt , in terms of the Dirac delta-function.

C. Coherent Sum of HHG Amplitudes: Many-molecule vs. One-molecule Signal

It is interesting also to consider the *total* amplitude $A_{tot.}(\Omega)$ of HHG emission from all the molecules interacting with the (probe laser) field. This is given by the *coherent* sum of the individual amplitudes emitted by the molecules at the positions \mathbf{X}_j for all $j = 1, 2, 3, \dots, \mathcal{N}$, where \mathcal{N} is the number of molecules in the interaction volume, or

$$\begin{aligned} A_{tot.}(\Omega) &\equiv \sum_{j=1}^{\mathcal{N}} A_j(\Omega) \\ &= \sum_n \left\{ \sum_{j=1}^{\mathcal{N}} e^{-i(\mathbf{K}_\Omega - n\mathbf{k}_\omega) \cdot \mathbf{X}_j} \right\}_1 \\ &\quad \times \left\{ -2\pi i \sum_n \delta(\Omega - n\omega) T_{i,i}(\Omega) \right\}_2 \end{aligned} \quad (27)$$

where we may identify the basic HHG transition matrix element for the emission of the n th harmonic per molecule as,

$$T_{i,i}(\Omega) = N_\Omega \epsilon_\Omega \cdot \tilde{\mathbf{D}}_{i,i}(\Omega) \quad (28)$$

It can be seen from Eq. (27) that the n th harmonic emission amplitude in fact factorizes into two parts, the first factor corresponds to the sum of the macroscopic space dependent phases associated with the random positions

\mathbf{X}_j of the *C.M.s* of the molecules in the interaction volume, and the second factor corresponds to the fundamental “one molecule” emission amplitude, independent of the position of the *C.M.s* of the molecules. The macroscopic phase factor is explicitly given by

$$\{\dots\}_1 \equiv \left\{ \sum_{j=1, \mathcal{N}} e^{-i(\mathbf{K}_\Omega - n\mathbf{k}_\omega) \cdot \mathbf{X}_j} \right\}_1 \quad (29)$$

For a large number of molecules in the interaction volume, $\mathcal{N} \gg 1$, the phase factor oscillates greatly and thus tends to average out to zero, *except* when the condition,

$$(\mathbf{K}_\Omega - n\mathbf{k}_\omega) = 0 \quad (30)$$

is fulfilled; in that case it yields the phase sum $\{\dots\}_1 = \mathcal{N}$. It is readily understood that the condition (30) corresponds exactly to the momentum conservation between the final momentum of the emitted harmonic photon, $\hbar\mathbf{K}_\Omega$, and the sum of the momenta of n laser photons, $n\hbar\mathbf{k}_\omega$. This is the phase-matching condition in the forward direction [37].

The probability of emission of the harmonics is given as usual by the absolute square of the total amplitude Eq. (27). Under the phase-matching condition the latter is therefore coherently *amplified* by a (generally large) factor of \mathcal{N}^2 . This is also the origin of the *quadratic* pressure dependence of the high harmonic signals, as well as their unusual strengths, that had been found in the very first experimental observations (e.g. [38, 39]).

The second factor $\{\dots\}_2$ gives the fundamental “one-molecule” quantum emission amplitude. We also note that if the absolute probability of the harmonic emission is needed then the proportionality factor $N_\Omega = \sqrt{\frac{2\pi\hbar\omega}{L^3}}$ becomes essential, and that for a given polarization direction of the emitted photon, ϵ_Ω , the projection of the dipole expectation value must be taken in that direction.

D. Continuous Medium and the Phase-matching Function

If one assumes that the gas molecules are distributed effectively continuously with a distribution function $\mathcal{N}\rho(\mathbf{R})d^3R$, where $\rho(\mathbf{R})$ is the so-called “density function per molecule”, then one may replace the sum over j in Eq. (29) by the integration over the interaction volume. Clearly, in this case the square of the macroscopic phase factor, $|\{\dots\}_1|^2$, takes the form

$$|\{\dots\}_1|^2 = \mathcal{N}^2 \mathcal{F}(\mathbf{K}_\Omega - n\mathbf{k}_\omega) \quad (31)$$

where,

$$\mathcal{F}(\mathbf{K}_\Omega - n\mathbf{k}_\omega) = \left| \int d^3X \rho(\mathbf{X}) e^{i(\mathbf{K}_\Omega - n\mathbf{k}_\omega) \cdot \mathbf{X}} \right|^2 \quad (32)$$

which is the so-called phase-matching function. It peaks for its argument near zero (near the forward direction), but falls off rapidly away from it.

E. Coherent Elastic vs. Incoherent Inelastic Transitions

Eqs. (30) and (27) show, respectively, that both the phase matching condition (momentum conservation) and the frequency matching condition (energy conservation) in the process ought to be fulfilled *simultaneously* in order that the macroscopic signal to be coherently amplified in space and time. As already noted earlier, the former condition leads to the directional coherence (forward propagation) of the HHG emission, while the latter implies the *elastic* nature of the accompanying molecular transitions for which the final (“recombination”) state f of the molecular system is the *same* as the initial state i , with $E_i = E_f$. In contrast, for an *inelastic* transition, $i \rightarrow f$, when $E_i \neq E_f$, there would be in general only “hyper-Raman” emissions, with frequencies $\Omega_{if} = (n'\omega - |E_i - E_f|)$, that are generally incommensurate with the incident laser frequency or its multiple, or the HHG frequency, $\Omega = n\omega$. Thus the non-vanishing relative phase difference $\Delta\phi \equiv (|E_i - E_f| - n\omega)t$ would fail to stimulate the hyper-Raman transitions by the incident field, unlike the stimulated spontaneous nature of the associated HHG. Also the non-vanishing momentum difference between hyper-Raman radiation and the multiple of the laser photons $\mathbf{K}_{\Omega_{if}} - n\mathbf{k}_\omega \neq 0$ makes the former macroscopically and directionally incoherent.

Finally, we note that the probability of the electronically inelastic processes associated with the transitions into the continuum (e.g. ionization) or between continua (e.g. inverse Bremsstrahlung [40]) that are commensurate with the emission of the n th harmonic at the “one-molecule” level, will be incoherent spatially, and therefore would enhance only proportional to the total number of molecules, \mathcal{N} , in the interaction volume. This is in stark contrast to the coherent amplification of the HHG emission at the n th harmonic, that is proportional to \mathcal{N}^2 .

F. Differential Rate of Coherent High Harmonic Generation

To derive the explicit expression for the probability of HHG per unit time i.e. the *rate* of generation of coherent high harmonics, we take the absolute square of the total HHG amplitude Eq. (27) and divide by the long observation time T , use a useful representation of the square of the delta-function ([2, p. R12]),

$$\delta^2(\Omega - n\omega) = \lim_{T \rightarrow \infty} \frac{T}{2\pi} \delta(\Omega - n\omega), \quad (33)$$

and sum over the emitted photon modes (with $\sum_{\mathbf{K}_\Omega} \equiv L^3 \int d\hat{\mathbf{K}}_\Omega \int dK_\Omega K_\Omega^2$) and get:

$$\begin{aligned} W(\Omega) &= \lim_{T \rightarrow \infty} \sum_{\mathbf{K}} \frac{|A_{tot.}(\Omega)|^2}{T} \\ &= \mathcal{N}^2 \sum_n \int d\hat{\mathbf{K}}_\Omega \mathcal{F}(\mathbf{K}_\Omega - n\mathbf{k}_\omega) \\ &\quad \times \int dW(n\omega) \end{aligned} \quad (34)$$

where,

$$\begin{aligned} dW(n\omega) &= 2\pi\delta(\Omega - n\omega)L^3 \\ &\quad \times \left| N_\Omega \epsilon_\Omega \cdot \tilde{\mathbf{D}}_{i,i}(n\omega) \right|^2 K_\Omega^2 dK_\Omega \end{aligned} \quad (35)$$

is the differential rate of HHG per molecule. Noting that the main contribution arises from the phase matching condition along the forward direction, we may carry out the mode-integrations to get:

$$W(n\omega) = 2\pi \left| T_{i,i}^{(n)} \right|^2 \frac{(n\omega)^2}{c^3} \quad (36)$$

where we have used, $K_\Omega \equiv \frac{\Omega}{c}$, $\mathbf{K}_\Omega \equiv K_\Omega \hat{\mathbf{K}}_\Omega$, and the fundamental transition matrix element for the emission of the n th harmonic, $T_{i,i}^{(n)}$, is given in terms of the $F.T.$ of the dipole expectation value $\tilde{\mathbf{D}}_{i,i}(n\omega)$ by:

$$T_{i,i}^{(n)} = \sqrt{2\pi(n\omega)} \epsilon_\Omega \cdot \tilde{\mathbf{D}}_{i,i}(n\omega) \quad (37)$$

for, $L^3 |N_\Omega|^2 = 2\pi(n\omega)$.

IV. EVALUATION OF “ONE MOLECULE” HHG AMPLITUDE

Clearly the dynamical properties of the HHG signal are given by the rate of HHG emission per molecule, Eq. (36), while the total signal is the same to within a proportionality constant given by the square of the number of molecules in the interaction volume, \mathcal{N}^2 , and the phase-matching constant $\int d\hat{\mathbf{K}}_\Omega \mathcal{F}(\mathbf{K}_\Omega - n\mathbf{k}_\omega)$ that peaks in the forward direction. We therefore proceed to evaluate the dynamical signal per molecule (in a relative scale) as follows: (i) solve the Schrödinger equation for the nuclear and the electronic motions of the interacting laser-molecule system, (ii) construct a complete set of orthonormal reference states, $|i\rangle \equiv |\chi_i(t)\rangle$, of the molecule, created by the pump pulse, (iii) determine their statistical weights according to the *one-to-one* correspondence with the thermally occupied rotational eigenstates of the ensemble, (iv) calculate the “one molecule” probability amplitude for HHG for each member of the ensemble of linearly independent reference states $|i\rangle$, using Eq. (36), and finally, (v) obtain the (scaled) signal “per molecule”

by thermally averaging the *probabilities* of HHG emission from each member of the ensemble of the reference states, using the distribution of their statistical weights.

In the Born-Oppenheimer approximation and non-overlapping pump and probe pulse condition, we may consider the evolution of the wavefunctions of the nuclear and the electronic parts separately and combine them together to obtain the wavefunction of the interacting system to evaluate the transition matrix elements of interest.

A. Pump Pulse Interaction and Rotational Wavepackets as Reference States

The nuclear rotational motion under the action of the pump pulse is determined by the Schrödinger equation governed by the partial Hamiltonian

$$H_N(t) + V_{N-L_1}(t), \quad (38)$$

i.e.

$$i \frac{\partial}{\partial t} \Phi_{JM}(t) = (H_N + V_{N-L_1}(t)) \Phi_{JM}(t). \quad (39)$$

We first construct the fundamental set of linearly independent solutions of Eq. (39), each evolving independently from each of the occupied rotational eigenstates $\{|J_0 M_0\rangle\}$. We expand it on the basis of the eigenstates $\{|JM\rangle\}$, as

$$\Phi_{J_0 M_0}(t) = \sum_{JM} C_{JM}^{(J_0 M_0)}(t) |JM\rangle e^{-iE_{JM}t} \quad (40)$$

The coefficients $C_{JM}^{(J_0 M_0)}(t)$ satisfy the system of coupled linear differential equations

$$i \frac{\partial}{\partial t} C_{JM}^{(J_0 M_0)}(t) = \sum_{J'M'} \langle JM | V_{N-L_1}(t) | J'M' \rangle C_{J'M'}^{(J_0 M_0)}(t) \quad (41)$$

This set of equations can be easily obtained (e.g. [41]) by projecting on a given eigenstate from the left. In practice we obtain the set of the fundamental solutions $|\Phi_{J_0 M_0}\rangle$ by numerical integration using the well-known Runge-Kutta method [34], starting with the following independent initial conditions:

$$C_{JM}^{(J_0 M_0)}(t_i) = \delta_{J,J_0} \delta_{M,M_0} \quad (42)$$

We may note explicitly here that (a) each independent wavepacket-state $|\Phi_{J_0 M_0}(t)\rangle$ evolves in *one-to-one* correspondence with the initially occupied rotational eigenstate $|J_0 M_0\rangle$. Taken together they form a complete set of orthonormal rotational wavepacket-states (linear superposition of rotational eigenstates):

$$\sum_{J_0 M_0} |\Phi_{J_0 M_0}(t)\rangle \langle \Phi_{J_0 M_0}(t)| = \mathbf{1} \quad (43)$$

In general a gas jet of molecules in a pump-probe experiment at a finite temperature T , is not in a pure quantum state but rather is in a state of thermal mixture of the rotational eigenstates, $\{|J_0 M_0\rangle\}$. We therefore introduce the quantum statistical mechanical device of a hypothetical ensemble of mutually independent and identical reference molecules, each of which occupies the electronic ground state and the rotational eigenstates $\{|J_0 M_0\rangle\}$, the latter with statistical weights $\rho(J_0 M_0)$, given by the Boltzmann distribution:

$$\rho(e, J_0 M_0) = (1)_e \times Z_P e^{-E_{J_0 M_0}/kT}, \quad (44)$$

where

$$Z_P = \sum_{J_0} (2J_0 + 1) e^{-E_{J_0}/kT} \quad (45)$$

is the rotational partition function; $E_{J_0 M_0} = J_0(J_0 + 1)hBc$, for all M_0 ; B stands for the rotational constant. We shall assume for the present purpose that the pump pulse is not too strong so that the change in the occupation probability of the ground electronic state after the pump pulse interaction is negligible and hence the ground electronic state at a time t before the interaction with the probe pulse evolves simply to $|\phi_e(t)\rangle = e^{-iE_e t} |\phi_e(0)\rangle$, where E_e is the ground state energy. (We may assume that electronically only the ground electronic state $|\phi_e(0)\rangle$ is occupied initially). Thus, the linearly independent reference states of the molecule, after the interaction of the pump pulse and immediately before the interaction with the probe pulse, can be written as the direct product of the nuclear rotational wavepacket states and the electronic ground state:

$$|\chi_i(t)\rangle \equiv |\Phi_{J_0 M_0}(t)\rangle |\phi_e(t)\rangle \quad i \equiv (e, J_0 M_0). \quad (46)$$

The reference density matrix describing the molecular ensemble prepared by the pump pulse takes the form:

$$\begin{aligned} \rho_{mol}(e, J_0 M_0) &= \sum_i |\chi_i(t)\rangle \rho(e, J_0 M_0) \langle \chi_i(t)| \\ &= |\phi_e(t)\rangle |\Phi_{J_0 M_0}(t)\rangle \rho(j_0 M_0) \\ &\quad \times \langle \Phi_{J_0 M_0}(t) | \langle \phi_e(t) | \end{aligned} \quad (47)$$

where, $i \equiv (e, J_0 M_0)$. The above ensemble of molecular states describes the effective “initial” condition of the system after the pump pulse, when the probe pulse arrives at the molecular at \mathbf{X}_j . To avoid any possible confusion regarding the presence of the “mixed-state” of the ensemble, and the “rotational coherence”, we may already point out explicitly that while the ensemble is characterized by the statistical occurrence of the orthonormal reference states $\{|\chi_{i=e, J_0 M_0}(t)\rangle\}$, each one of these states carries the information of the rotational coherence induced by the pump pulse, as coded in the individual rotational wavepackets $\{|\Phi_{J_0 M_0}(t)\rangle\}$. Thus, when the thermal average of the HHG emission signal must be taken with respect to the *probability* of emission from

each member of the ensemble (as required by quantum statistical mechanics), it can not, and will not, wash out the rotational coherence that is present within each of them individually.

B. Interaction with Probe-Pulse and Evolution of the Electronic State

To proceed further, we next consider the evolution of the electronic state, governed by the partial Hamiltonian

$$H_e + V_{e-L_2}(t - t_d). \quad (48)$$

It is obtained conveniently from the knowledge of the electronic Green's function $G_e(t, t')$ [20] associated with the above Hamiltonian and defined by the inhomogeneous equation:

$$\left\{ i \frac{\partial}{\partial t} - (H_e + V_{e-L_2}(t - t_d)) \right\} G_e(t, t') = \delta(t - t') \mathbf{1}. \quad (49)$$

A solution of the above equation can be written as (in the strong-field KFR-approximation):

$$G_e(t, t') = -i\theta(t - t') \sum_{j, \mathbf{p}} \left| \phi_j^{(+)} \right\rangle e^{-iE_j^+ t} \left| \mathbf{p}(t - t_d) \right\rangle \times e^{-\frac{i}{2} \int_{t'-t_d}^{t-t_d} p^2(u) du} \times \left\langle \mathbf{p}(t' - t_d) \right| e^{iE_j^+ t'} \left\langle \phi_j^{(+)} \right| \quad (50)$$

where j runs over all the ionic electronic states $\left| \phi_j^{(+)} \right\rangle$, with eigenvalues E_j^+ , of the molecular ion and \mathbf{p} is the free momentum of the electron; $\mathbf{p}(t)$ stands for the instantaneous momentum in the presence of the field, defined as $\mathbf{p}(t) \equiv \left(\mathbf{p} + \frac{\mathbf{A}(t)}{c} \right)$. The validity of Eq. (50) (within the Born-Oppenheimer and KFR approximation) can be verified by substituting it in Eq. (49) and using the completeness relation

$$\sum_{\mathbf{p}} \langle \mathbf{r} | \phi_{\mathbf{p}}(t) \rangle \langle \phi_{\mathbf{p}}(t) | \mathbf{r} \rangle = \mathbf{1} \quad (51)$$

of the Volkov wavefunctions defined by:

$$\langle \mathbf{r} | \phi_{\mathbf{p}}(t) \rangle = e^{i\mathbf{p}(t) \cdot \mathbf{r}} e^{-\frac{i}{2} \left(\int^t p^2(u) du \right)} \quad (52)$$

as well as the completeness relation of the ionic states

$$\sum_j \left| \phi_j^{(+)} \right\rangle \left\langle \phi_j^{(+)} \right| = \mathbf{1} \quad (53)$$

We should note that the ionic states are generally much more tightly bound than the active electron in the highest occupied molecular orbital (HOMO). Thus in deriving G_e above, we have further neglected the change in the ionic states due the interaction with the probe pulse, which we may refer to as “bare-ion” approximation.

Finally, using Eqs. (43) and (50) we obtain the total Green's function $G_0(t, t')$ of the interacting system:

$$G_0(t, t') = -i\theta(t - t') \sum_{j, \mathbf{p}, JM} \left| \phi_j^{(+)} \right\rangle \left| \phi_{\mathbf{p}}(t - t_d) \right\rangle \times \left| \Phi_{JM}(t) \right\rangle e^{-iE_j^+(t-t')} \left\langle \Phi_{JM}(t') \right| \times \left\langle \phi_{\mathbf{p}}(t' - t_d) \right| \left\langle \phi_j^{(+)} \right| \quad (54)$$

The above Green's function of the system (54) therefore holds under (a) the adiabatic Born-Oppenheimer, (b) the strong-field KFR and (c) the “bare-ion” approximations.

C. The Total Wavefunction in Strong-Field Molecular KFR-approximation

Combining the Eqs. (17) and (46), we obtain the total intense-field molecular wavefunction at the lowest order strong field KFR-approximation:

$$|\Psi_i(t)\rangle = |\chi_i(t)\rangle + \int_{-\infty}^{\infty} dt' \times G_0(t, t') V_{e-L_2}(t' - t_d) |\chi_i(t')\rangle \quad (55)$$

where,

$$|\chi_i(t)\rangle = |\phi_e(t)\rangle |\Phi_{J_0 M_0}(t)\rangle \quad (56)$$

is a member of the ensemble of reference states of interest.

D. Evaluation of the Dipole Expectation Value

In the above we have obtained the necessary ingredients for evaluating the expectation of the dipole operator Eq. (23) explicitly. Substituting Eqs. (54) and (55) in Eq. (23), we get:

$$\begin{aligned} D_{i,i}(t) &= \left\langle \chi_i(t) \right| \hat{\mathbf{d}}_e \left| \Psi_i^{(1)}(t) \right\rangle + c.c. \\ &= \left\{ -i \int_{-\infty}^t dt' \langle \phi_e(t) | \langle \Phi_{J_0 M_0}(t) | \hat{\mathbf{d}}_e \right. \\ &\quad \times \sum_{j, \mathbf{p}, JM} \left| \phi_j^{(+)} \right\rangle \left| \phi_{\mathbf{p}}(t - t_d) \right\rangle \\ &\quad \times \left| \Phi_{JM}(t) \right\rangle e^{-iE_j^+(t-t')} \left\langle \Phi_{JM}(t') \right| \\ &\quad \times \left\langle \phi_{\mathbf{p}}(t' - t_d) \right| \left\langle \phi_j^{(+)} \right| \\ &\quad \times V_{e-L_2}(t' - t_d) \left| \Phi_{J_0 M_0}(t') \right\rangle \left| \phi_e(t') \right\rangle \left. \right\} \\ &\quad + c.c. \end{aligned} \quad (57)$$

To simplify the expression further we (i) change the variable $t' \rightarrow t' + t_d$, and similarly, $t \rightarrow t + t_d$; (ii) note that the free evolution of the rotational wavepacket after the interaction with the pump pulse at $(t + t_d)$

is $\Phi_{J_0 M_0}(t+t_d) = e^{-iH_N t} \Phi_{J_0 M_0}(t_d)$, and similarly, at $(t'+t_d)$, $\Phi_{J_0 M_0}(t'+t_d) = e^{-iH_N t'} \Phi_{J_0 M_0}(t_d)$, (iii) the time dependence of the unperturbed initial electronic state at $\phi_e(t+t_d) = |\phi_e\rangle e^{-iE_i(t+t_d)}$, and similarly for the ionic states, $\phi_j^{(+)}(t+t_d) = |\phi_j^{(+)}\rangle e^{-iE_j^{+}(t-t_d)}$, (v) introduce the overlaps (“Dyson-orbitals”),

$$|\phi_e^{(j)}\rangle = \langle \phi_j^{(+)}(1, 2, \dots, N_e - 1) | \phi_e(1, 2, \dots, N - 1, N) \rangle \quad (58)$$

and retain only the (dominant) contribution from the lowest lying ionic state ($j = 0$), to obtain:

$$\begin{aligned} D_{i,i}(t) = & -i \sum_{jJM,\mathbf{p}} \langle \Phi_{J_0 M_0}(t) | \langle \phi_e^{(0)} | \hat{\mathbf{d}}_e | \\ & \times |\mathbf{p}(t-t_d)\rangle | \phi_j^{+} \rangle | \Phi_{JM}(t) \rangle \\ & \times \int_{-\infty}^t dt' e^{-i(E_j^{+}-E_0)(t-t')} \\ & \times e^{-i \int_{t'-t_d}^{t-t_d} (\mathbf{p}(u)^2/2) du} \\ & \times \langle \Phi_{JM}(t') | \langle \phi_j^{+} | \langle \mathbf{p}(t'-t_d) | \\ & \times | V_{e-L_2}(t'-t_d) | \phi_e^{(0)} \rangle | \Phi_{J_0 M_0}(t') \rangle \\ & + c.c. \end{aligned} \quad (59)$$

Or,

$$D_{i,i}(t) = \langle \Phi_{J_0 M_0}(t) | D_e(t) | \Phi_{J_0 M_0}(t) \rangle, \quad (60)$$

where clearly the electronic part of the expectation value is given by the integral

$$\begin{aligned} D_e(t) = & \left\{ -i \sum_{\mathbf{p}} \langle \phi_e^{(0)} | \hat{\mathbf{d}}_e | \mathbf{p}(t) \rangle \right. \\ & \times \int_{-\infty}^{t_d+t} dt' e^{-i \int_{t'}^t (\mathbf{p}(u)^2/2 + E_B) du} \\ & \times \langle \mathbf{p}(t') | -\mathbf{F}(t') \cdot \hat{\mathbf{d}}_e | \phi_e^{(0)} \rangle \left. \right\} + c.c. \end{aligned} \quad (61)$$

where, $\mathbf{F}(t)$ is the probe field. Finally, by using the rate of emission of the n th harmonic as given by Eq. (36), we obtain the dynamic HHG signal, for a pump-probe delay time t_d ,

$$\begin{aligned} S^{(n)}(t_d, \alpha) = & 2\pi \sum_{J_0 M_0} \rho(J_0) \left| \langle \Phi_{J_0 M_0}(t_d) | T_e^{(n)}(\theta, \phi; \alpha) | \right. \\ & \times \left. | \Phi_{J_0 M_0}(t_d) \rangle \right|^2 \frac{(n\omega)^2}{c^3} \end{aligned} \quad (62)$$

where $(\theta, \phi) \equiv \hat{\mathbf{R}}_N$ is the orientation of the molecular axis in space and $T_e^{(n)}(\theta, \phi; \alpha)$ is a *HHG transition operator*.

E. Derivation of the HHG operator $T^{(n)}(\theta, \phi; \alpha)$

We shall now proceed to derive an explicit expression of the HHG transition operator $T_e^{(n)}(\theta, \phi; \alpha)$ for an ar-

bitrary relative angle α between the linear polarization directions of the pump and the probe pulse. To this end, we first consider the most common experimental geometry in which the pump and probe polarizations are chosen to be parallel.

1. HHG operator: Parallel polarization $\alpha = 0$

We recall that for a linearly polarized probe pulse $\mathbf{F}_2(t) = \epsilon_{\hat{\Omega}} F(t) \cos \omega t$, the corresponding vector potential is

$$\mathbf{A}(t) = -\epsilon_{\hat{\Omega}} \left(\frac{cF(t)}{\omega} \right) \sin \omega t \quad (63)$$

It is convenient in this case to take the space fixed polar axis (z -axis) along the common direction of the polarizations $\epsilon_1 \parallel \epsilon_2 \parallel \hat{\mathbf{z}}$. To evaluate the tripe-integral over the intermediate momenta \mathbf{p} in Eq. (61) we employ the stationary phase method [42], with the stationary values

$$\mathbf{p}_{st}(t, t') = \frac{1}{t-t'} \int_{t'}^t \mathbf{A}(t'') dt'', \quad (64)$$

for which the derivative of the action $S(t, t')$ with respect to $t' = t - \tau$ is equal to zero. The corresponding stationary value of the action is,

$$S_{st}(t, t') = \int_{t'}^t \left\{ \frac{1}{2} \left(\mathbf{p}_{st}(t, t'') - \frac{1}{c} \mathbf{A}(t'') \right)^2 + E_B \right\} dt'', \quad (65)$$

where, $\mathbf{p}(t) = \mathbf{p}_{st}(t, t') - \frac{1}{c} \mathbf{A}(t)$ and $\mathbf{p}(t') = \mathbf{p}_{st}(t, t') - \frac{1}{c} \mathbf{A}(t')$. Thus, projecting the resulting value of $D_e(t)$ on to the polarization direction ϵ_{Ω} of the emitted harmonic we get,

$$\begin{aligned} D_e(t) = & \left\{ i \int_0^t dt' \left(\frac{\pi}{\epsilon + i(t-t')/2} \right)^{3/2} \right. \\ & \times \langle \phi_e^{(0)} | \epsilon_{\Omega} \cdot \mathbf{r} | \mathbf{p}(t) \rangle e^{-iS_{st}(t, t')} \\ & \times \left. \langle \mathbf{p}(t') | \mathbf{F}(t') \cdot \mathbf{r} | \phi_e^{(0)} \rangle \right\} + c.c. \end{aligned} \quad (66)$$

We may note that the first matrix element in this expression (reading from the right to the left) corresponds to the “ionization” transition at time t' , $d_{ion}(t') \equiv \langle \mathbf{p}(t') | \mathbf{F}(t') \cdot \mathbf{r} | \phi_e^{(0)} \rangle$, whereas the last matrix element corresponds to a “recombination” transition of the electron back to the same initial state at a time t , $d_{rec}(t) \equiv \langle \phi_e^{(0)} | \epsilon_{\Omega} \cdot \mathbf{r} | \mathbf{p}(t) \rangle$. The interval $(t-t')$ corresponds to the intermediate time that the electron spends in the continuum Volkov states, between the absorption of n photons in the first step and the emission of the harmonic frequency $\Omega = n\omega$ in the last step. We have assumed that there was no significant depletion of the ground state population during the process. However, if needed, a

weak depletion due to ionization could be accounted for without difficulty by introducing in the above expression the exponential decay factor: $e^{-(\gamma/2)(t+t')}$, where γ is the total ionization rate.

2. The “ionization” and “recombination” matrix elements

To evaluate the matrix elements of “ionization” and “recombination” in Eq. (66), we assume that the wavefunction of the active electron may be given by the highest occupied molecular orbital or HOMO. This can be written either in the multi-center LCAO-MO form, or, by transforming it into an equivalent single-center-MO (by appropriate transformations, e.g. [43, 44]). It is useful also to note that in the latter form, it often suffices for problems of interaction of molecules with long-wavelength laser fields, and in conjunction with the “length gauge”, to retain only the asymptotic limit of the orbitals at distances away from the molecular center.

In general, let the unperturbed MO of the active electron of a linear molecule, in the Born-Oppenheimer approximation, be given in the body fixed frame by the single-center expansion:

$$\phi_e^{(0)}(\mathbf{r}) = \sum_l C_l^{(m)} R_l(r) Y_{lm}(\hat{\mathbf{r}}) \quad (67)$$

where $C_l^{(m)}$ are the expansion coefficients (at a given internuclear separation R), $R_l(r)$ are the radial waves of angular momentum l , $Y_{lm}(r)$ are the spherical harmonics, and m is the projection of the angular momentum of the active electron along the molecular axis, that is conserved and hence also characterizes the MO.

Next, we transform the molecular orbitals Eq. (67) from the body fixed frame to the space fixed frame by using the Wigner transformation \mathbf{D} ,

$$\begin{aligned} \phi_e^{(0)}(\mathbf{r}) &= \hat{\mathbf{D}} \phi_e^{(0)}(\mathbf{r}) \\ &= \sum_l C_l^{(m)} R_l(r) \\ &\quad \times \sum_\mu D_{\mu m}^l(\phi, \theta, \chi) Y_{l\mu}(\hat{\mathbf{r}}) \end{aligned} \quad (68)$$

Above $D_{\mu m}^l(\phi, \theta, \chi) = e^{-i\mu\phi} d_{\mu m}^l(\theta) e^{-im\chi}$ is the Wigner rotation matrix where (ϕ, θ, χ) are the Euler’s angles which define the orientation of the molecular axis to the space fixed coordinate frame [45]. The middle term of the Wigner matrix, $d_{\mu m}^l(\theta)$, have been tabulated e.g. in reference [45, 46]. The matrix element of the dipole along the direction of the probe pulse, appearing in Eq. (66), then reads:

$$\begin{aligned} d_{ion}(t') &= F(t') \sum_l C_l^{(m)} \sum_\mu D_{\mu m}^l(\phi, \theta, \chi) \\ &\quad \times \langle e^{i\mathbf{p}_{t'} \cdot \mathbf{r}} | \epsilon_\omega \cdot \mathbf{r} | R_l(r) Y_{lm}(\hat{\mathbf{r}}) \rangle \end{aligned} \quad (69)$$

Further, we expand $e^{i\mathbf{p}_{t'} \cdot \mathbf{r}}$ in spherical harmonics,

$$\begin{aligned} e^{i\mathbf{p}_{t'} \cdot \mathbf{r}} &= \frac{2\pi}{\sqrt{p_{t'} r}} \sum_{l' m'} (i)^{l'} J_{l'+1/2}(p_{t'} r) \\ &\quad \times Y_{l' m'}(\hat{\mathbf{p}}_{t'}) Y_{l' m'}(\hat{\mathbf{r}}) \end{aligned} \quad (70)$$

and note that in this system of axes we have,

$$\epsilon_\omega \cdot \mathbf{r} = r \sqrt{\frac{4\pi}{3}} Y_{10}(\hat{\mathbf{r}}) \quad (71)$$

Note also that the instantaneous momentum $\mathbf{p}_{t'}$ can be either parallel or anti-parallel with respect to the direction of the field so that $\theta_{p_t} = 0, \pi$ and $\phi_{p_t} = 0$. Therefore, the spherical harmonics with the argument $\hat{\mathbf{p}}_{t'}$ can be simplified to $Y_{l' m'}(\hat{\mathbf{p}}_{t'}) = (\sigma)^{l'} \sqrt{\frac{2l'+1}{4\pi}} \delta_{m', 0}$, with $\sigma = 1$ for $\theta_{p_t} = 0$ and $\sigma = -1$ for $\theta_{p_t} = \pi$. Substituting Eqs. (70) and (71) in Eq. (69) we obtain (with $l' = l_i$),

$$d_{ion}(t') = F(t') \sum_{l_i} C_{l_i}^{(m)} D_{m0}^{l_i}(\phi, \theta, \chi) \beta_{ion}(l_i, m; t') \quad (72)$$

$$\begin{aligned} \beta_{ion}(l_i, m; t') &= \frac{(2\pi)^{3/2}}{\sqrt{3p_{t'}}} \sum_l (i\sigma)^l \sqrt{(2l+1)} \\ &\quad \times \langle l_i 0 | 10 | l \mu \rangle I_{l_i, l}(t') \end{aligned} \quad (73)$$

where, we have defined the radial integrals (m fixed) by

$$I_{l_i, l}(t') = \int_0^\infty J_{l+\frac{1}{2}}(p_{t'} r) R_{l_i}^m(r) r^{-1/2} r^2 dr \quad (74)$$

Using the Slater orbitals representation of the single center radial functions, $R_l(r) = r^{\eta-1} e^{-\alpha r}$, the radial integrals (I ’s) appearing in d_{ion} (Eq. (72)) can be evaluated explicitly by using the formula [47]

$$\begin{aligned} \int_0^\infty e^{-\alpha x} J_\nu(\beta x) x^{\mu-1} dx &= \frac{\left(\frac{\beta}{2}\right)^\nu \Gamma(\nu + \mu)}{\sqrt{(\alpha^2 + \beta^2)^{\nu+\mu}} \Gamma(\nu + 1)} \\ &\quad \times F\left(\frac{\nu + \mu}{2}, \frac{1 - \mu + \nu}{2}, \right. \\ &\quad \left. \nu + 1; \frac{\beta^2}{\alpha^2 + \beta^2}\right) \end{aligned} \quad (75)$$

where $F(a, b, c; x)$ is a hypergeometric function. Note that since the argument $x \equiv \frac{\beta^2}{\alpha^2 + \beta^2} < 1$ the hypergeometric function is guaranteed to converge for all values of a , b , and c . For ionization step, the radial integration

reads

$$\begin{aligned}
I_{l_i, l_i+1}(t') &= \frac{\left(\frac{p_{t'}}{2}\right)^{l_i+3/2} \Gamma(l_i + Z_c/p_B + 4)}{\sqrt{(P_B^2 + p_{t'}^2)^{l_i+Z_c/p_B+4}} \Gamma(l_i + \frac{5}{2})} \\
&\times F\left(\frac{l_i + Z_c/p_B + 4}{2}, \frac{l_i - Z_c/p_B}{2}, \right. \\
&\quad \left. l_i + \frac{5}{2}; \frac{p_{t'}^2}{p_B^2 + p_{t'}^2}\right) \\
I_{l_i, l_i-1}(t') &= \frac{\left(\frac{p_{t'}}{2}\right)^{l_i-1/2} \Gamma(l_i + Z_c/p_B + 2)}{\sqrt{(P_B^2 + p_{t'}^2)^{l_i+Z_c/p_B+2}} \Gamma(l_i + \frac{1}{2})} \\
&\times F\left(\frac{l_i + Z_c/p_B + 2}{2}, \frac{l_i - Z_c/p_B - 2}{2}, \right. \\
&\quad \left. l_i + \frac{1}{2}; \frac{p_{t'}^2}{p_B^2 + p_{t'}^2}\right) \quad (76)
\end{aligned}$$

Exactly the same expressions hold for the radial integrals appearing in the recombination dipole $d_{rec}(l_r, m; t)$ (except that l_i is changed to l_r , and t' to t , in Eq. (76)), throughout.

The Clebsch-Gordan coefficient in Eq. (73) implies that only the $\mu = 0$ term and $l = l_i \pm 1$ terms survive in the sums and we get for the ionization dipole,

$$d_{ion}(t') = F(t') \sum_{l_i} C_{l_i}^{(m)*} D_{m0}^{(l_i)}(\phi, \theta, \chi) \beta_{ion}(l_i, m; t') \quad (77)$$

with

$$\begin{aligned}
\beta_{ion}(l_i, m; t') &= \frac{2\pi}{\sqrt{2p_{t'}}} \sqrt{(2l_i + 1)} \\
&\times ((i\sigma)^{l_i+1} (l_i + 1) I_{l_i, l_i+1}(t') \\
&+ (i\sigma)^{l_i-1} l_i I_{l_i, l_i-1}(t')) \quad (78)
\end{aligned}$$

In the above we have introduced the angular momentum notation l_i for the initial bound state in the “ionization” matrix element (and l_r , in the “recombination” matrix element).

We may assume that the emitted harmonic is observed with its polarization along the same direction as the probe pulse polarization. (There is no difficulty, except lengthier algebra, to obtain the expression for the polarization direction orthogonal to it, but the former would give the dominant contribution under phase matching condition. Following an analogous calculation as above we get the “recombination” matrix element as:

$$d_{rec}(t) = \sum_{l_r} C_{l_r}^{(m)*} D_{0m}^{l_r*}(\phi, \theta, \chi) \beta_{rec}(l_r, m; t') \quad (79)$$

with

$$\begin{aligned}
\beta_{rec}(l_r, m; t) &= \frac{2\pi}{\sqrt{2p_t}} \sqrt{(2l_r + 1)} \\
&\times ((i\sigma)^{l_r+1} (l_r + 1) I_{l_r, l_r+1}(t) \\
&+ (i\sigma)^{l_r-1} l_r I_{l_r, l_r-1}(t)) \quad (80)
\end{aligned}$$

Substituting Eqs. (77-78) and (79-80) in Eq. (66), we obtain

$$\begin{aligned}
D_e(t) &= i \sum_{l_i, l_r} d_{0m}^{l_r}(\theta) d_{0m}^{l_i}(\theta) \\
&\times [C_{l_r}^{(m)*} C_{l_i}^{(m)} M_e(t) + c.c.] \quad (81)
\end{aligned}$$

where we have used the relation

$$D_{m0}^{l_r*}(\phi, \theta, \chi) D_{m0}^{l_i}(\phi, \theta, \chi) = d_{0m}^{l_r}(\theta) d_{0m}^{l_i}(\theta) \quad (82)$$

and defined the radial integral,

$$\begin{aligned}
M_e(t) &= i \int_{-\infty}^{t_d+t} dt \left(\frac{\pi}{(\epsilon + i(t-t')/2)} \right)^{3/2} \\
&\times \beta_{rec}(l_r, m; t) e^{-iS_{st}(t, t')} \\
&\times F(t') \beta_{ion}(l_i, m; t') \quad (83)
\end{aligned}$$

Next, by integrating over t' , taking the Fourier transform with respect to t , we obtain (cf. Eq.(28)), the HHG operator $T_e^{(n)}(\theta, \phi; 0)$ for the n th harmonic generation:

$$\begin{aligned}
T_e^{(n)}(\theta, \phi; 0) &= \sqrt{2\pi(n\omega)} \tilde{D}_e(n\omega) \\
&= \sqrt{2\pi(n\omega)} \sum_{l_i, l_r} d_{0m}^{l_r}(\theta) d_{0m}^{l_i}(\theta) \\
&\times \tilde{\alpha}_{zz}^{(n)}(l_r, l_i; m) \quad (84)
\end{aligned}$$

where, $\tilde{\alpha}_{zz}^{(n)}(l_r, l_i; m)$ is given by the n th Fourier coefficient of $D_e(t)$:

$$\begin{aligned}
\tilde{\alpha}_{zz}^{(n)}(l_r, l_i; m) &\equiv \\
&F.T. [C_{l_r}^{(m)*} C_{l_i}^{(m)} M_e(t) + c.c.] (n\omega) \quad (85)
\end{aligned}$$

Next, by substituting Eq. (84) in Eq. (62), we obtain the rotational matrix elements,

$$\langle \Phi_{J_0 M_0}(t_d) | d_{0m}^{l_r}(\theta) d_{0m}^{l_i}(\theta) | \Phi_{J_0 M_0}(t_d) \rangle, \quad (86)$$

which can be evaluated directly by using the tabulated values of the $d_{0m}^l(\theta)$ given by elementary trigonometric functions (see, Tab. I). Alternatively, we may first combine the product

$$\begin{aligned}
d_{0m}^{l_r}(\theta) d_{0m}^{l_i}(\theta) &= \sqrt{\frac{4\pi}{2l_r+1}} (-1)^m Y_{l_r, -m}(\theta, \phi) \\
&\sqrt{\frac{4\pi}{2l_i+1}} Y_{l_i, m}(\theta, \phi) \\
&= \sum_{L=|l_r-l_i|}^{l_r+l_i} (-1)^m \langle l_r, l_i, -m, m | L, 0 \rangle \\
&\times \langle l_r, l_i, 0, 0 | L, 0 \rangle P_L(\cos \theta) \quad (87)
\end{aligned}$$

and we obtain

$$T_e^{(n)}(\theta, \phi; 0) = \sum_{l_i, l_r, L} \tilde{a}_{zz}^{(n)}(l_r, l_i, L; m) P_L(\cos \theta) \quad (88)$$

where,

$$\begin{aligned} \tilde{a}_{zz}^{(n)}(l_r, l_i, L; m) &= \sqrt{2\pi(n\omega)} \tilde{\alpha}_{zz}^{(n)}(l_r, l_i; m) \\ &\times (-1)^m \langle l_r, l_i, -m, m | L, 0 \rangle \\ &\times \langle l_r, l_i, 0, 0 | L, 0 \rangle. \end{aligned} \quad (89)$$

Thus, the expectation value of the transition operator with respect to the rotational wavepacket can be obtained more elegantly in terms of the Legendre polynomials moments:

$$\langle P_L \rangle_{J_0 M_0}(t_d) \equiv \langle \Phi_{J_0 M_0}(t_d) | P_L(\theta) | \Phi_{J_0 M_0}(t_d) \rangle \quad (90)$$

Finally, by substituting the above relations (Eq. (88)) in Eq. (62), and taking the statistical average over the ensemble of the emission probabilities from the ensemble of rotational wavepackets, we obtain the HHG signal (i.e. the rate per unit time of generation of the n th harmonic per molecule) in the special case of parallel polarizations (cf. [19]):

$$\begin{aligned} S^{(n)}(t_d; 0) &= 2\pi \sum_{J_0 M_0} \rho(J_0) \left| \sum_{L, l_r, l_i} \tilde{a}_{zz}^{(n)}(l_r, l_i, L; m) \right. \\ &\quad \left. \times \langle P_L \rangle_{J_0 M_0}(t_d) \right|^2 \frac{(n\omega)^2}{c^3} \end{aligned} \quad (91)$$

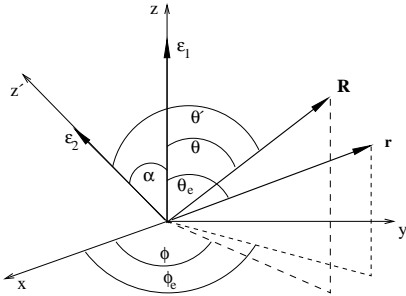


Figure 3: A schematic diagram defining: molecular axis \mathbf{R} , electron position \mathbf{r} , pump polarization ϵ_1 , and probe polarization ϵ_2 ; α is the operational laboratory angle.

F. General Polarization Geometry: Arbitrary α

So far we have assumed that the pump and the probe polarizations are parallel and that they point along the space fixed polar axis \hat{z} . In the general case, we may define, without loss of generality, the relative angle between the polarizations, α , to lie in the $(z - z' - x)$ -plane (cf. Fig. 3). From the figure, it can be seen that we simply need to re express the direction of the molecular axis, (θ, ϕ) , given with respect to the pump polarization $\epsilon_1 \parallel \hat{z}$, in terms of the direction (θ', ϕ') with respect to the probe polarization direction $\epsilon_2 \parallel \hat{z}$. This is readily

achieved by simply replacing $\cos \theta \rightarrow \cos \theta'$, and using the well known relation

$$\cos \theta' = \cos \alpha \cos \theta + \sin \theta \sin \alpha \cos \phi \quad (92)$$

or the vector addition coefficients and the addition theorem

$$P_L(\cos \theta') = \frac{4\pi}{2L+1} Y_{L,M}(\theta, \phi) Y_{L,M}^*(\alpha, 0). \quad (93)$$

Thus, we obtain the general expression of the HHG operator for any α [20]:

$$\begin{aligned} T_e^{(n)}(\theta', \phi'; \alpha) &= \sqrt{2\pi(n\omega)} \sum_{l_i, l_r} d_{0,m}^{l_r}(\theta') d_{0,m}^{l_i}(\theta') \\ &\quad \times \tilde{a}_{zz}^{(n)}(l_r, l_i; m). \end{aligned} \quad (94)$$

Or,

$$\begin{aligned} T_e^{(n)}(\theta', \phi'; \alpha) &= \sum_{l_r, l_i, L, M} \tilde{a}_{zz}^{(n)}(l_r, l_i, L; m) P_L(\cos \theta') \\ &= \sum_{LM} \sum_{l_r, l_i} \tilde{a}_{zz}^{(n)}(l_r, l_i, L; m) \\ &\quad \times \frac{4\pi}{2L+1} Y_{L,M}(\theta, \phi) Y_{L,M}^*(\alpha, 0) \end{aligned} \quad (95)$$

where $\tilde{a}_{zz}^{(n)}(l_r, l_i, L; m)$ is given by Eq. (89).

It is should be noted that, in general, if the molecular orbital coefficients were assumed to be complex,

$$C_l^{(m)} \equiv |C_l^{(m)}| e^{i\phi_l}, \quad (96)$$

then we should rewrite the dynamic parameters $\tilde{\alpha}_{zz}^{(n)}(l_r, l_i; m)$

(Eq.(85)) as:

$$\begin{aligned} \tilde{\alpha}_{zz}^{(n)}(l_r, l_i; m) &= F.T. \left[C_{l_r}^{(m)*} C_{l_i}^{(m)} M_e(t) + c.c. \right] \\ &= 2 |C_{l_r}^{(m)}| |C_{l_i}^{(m)}| \left[\cos \phi_{l_i l_r} \tilde{u}_{l_r, l_i, m}^{(n)} \right. \\ &\quad \left. - \sin \phi_{l_i l_r} \tilde{v}_{l_r, l_i, m}^{(n)} \right] \end{aligned} \quad (97)$$

where,

$$\phi_{l_i l_r} \equiv (\phi_{l_i} - \phi_{l_r}). \quad (98)$$

$M_e(t)$ is given by Eq. (83), and we have defined,

$$\tilde{u}_{l_r, l_i, m}^{(n)} = F.T. [Re \{M_e(t)\}] (n\omega) \quad (99)$$

$$\tilde{v}_{l_r, l_i, m}^{(n)} = F.T. [Im \{M_e(t)\}] (n\omega) \quad (100)$$

Thus, finally, we can express the general transition matrix element for the n th order harmonic as an expansion in Legendre polynomials in $\cos \alpha$, and the corresponding Legendre moments of the time-dependent axis distribution of the molecule:

$$\begin{aligned}
T^{(n)}(t_d, \alpha) &= \langle \Phi_{J_0 M_0}(t_d) | T^{(n)}(\theta, \phi; \alpha) | \Phi_{J_0 M_0}(t_d) \rangle \\
&= \sum_{L, l_r, l_i} \sqrt{2\pi(n\omega)} \left[\cos(\phi_{l_i, l_r}) \tilde{u}_{l_i, l_r, m}^{(n)} \right. \\
&\quad \left. - \sin(\phi_{l_i, l_r}) \tilde{v}_{l_i, l_r, m}^{(n)} \right] 2|C_{l_r}^{(m)}| |C_{l_i}^{(m)}| \\
&\quad \times (-1)^m \langle l_r, l_i, -m, m; L, 0 \rangle \\
&\quad \times \langle l_r, l_i, 0, 0; L, 0 \rangle \\
&\quad \times \langle P_L \rangle_{J_0 M_0}(t_d) P_L(\cos \alpha) \quad (101)
\end{aligned}$$

where, we have taken the expectation value of the HHG operator with respect to the rotational wavepacket $|\Phi(t_d)\rangle$, to obtain

$$\begin{aligned}
\frac{4\pi}{2L+1} \langle \Phi_{J_0 M_0}(t_d) | Y_{LM}(\theta, \phi) | \Phi_{J_0 M_0}(t_d) \rangle \\
= \langle P_L \rangle_{J_0 M_0}(t_d) P_L(\cos \alpha) \delta_{M,0} \quad (102)
\end{aligned}$$

This follows from the observation that the magnetic quantum numbers of all the rotational eigenstates in the individual wavepackets have the same value M_0 . It holds when the interaction operator $V_{e-L_2}(t)$ does not depend on the azimuth angle of the molecular axis in the body fixed frame. In the above expression, we have also used the relation $\sqrt{\frac{4\pi}{2L+1}} Y_{L0}(\theta, \phi) = P_L(\cos \theta)$, and an analogous relation with respect to the angle α , to simplify.

It is useful to note also that, if the orbital expansion coefficients are real, as is often the case, then $\phi_{l_i, l_r} = (0, \pi)$ and therefore the quantity in the square brackets in Eq. (101) simplifies to $[\dots] = [\cos(\phi_{l_i, l_r}) \tilde{u}_{l_i, l_r, m}^{(n)}]$ only.

G. A General Formula for the HHG Signal

Thus, finally, we substitute Eq. (101) in Eq. (91) and obtain the desired general expression (cf. [20]) for the n th harmonic signal from a linear molecule, for any value of t_d and α :

$$\begin{aligned}
S^{(n)}(t_d, \alpha) &= \sum_{J_0 M_0} \rho_{J_0 M_0} 2\pi \left| \sum_{L, l_r, l_i} \left[\cos \phi_{l_i, l_r} \tilde{u}_{l_i, l_r, m}^{(n)} \right. \right. \\
&\quad \left. \left. - \sin \phi_{l_i, l_r} \tilde{v}_{l_i, l_r, m}^{(n)} \right] 2|C_{l_r}^{(m)}| |C_{l_i}^{(m)}| \right. \\
&\quad \times (-1)^m \langle l_r, l_i, -m, m; L, 0 \rangle \\
&\quad \times \langle l_r, l_i, 0, 0; L, 0 \rangle \\
&\quad \times \langle P_L \rangle_{J_0 M_0}(t_d) P_L(\cos \alpha) \Big|^2 \\
&\quad \times \frac{(n\omega)^3}{c^3} \quad (103)
\end{aligned}$$

We may conclude the section by noting that for the special case of parallel polarizations, $\alpha = 0$, $P_L(\cos 0) = P_L(1) = 1$, Eq. (103) correctly goes over to the signal obtained for that special case, Eq. (91) (cf. [19]).

Table I: Explicit form of $d_{0m}^l(\theta)$ required for evaluating Eq. (84) [45, 46]

l	N ₂ ($m=0$)	O ₂ ($m=1$)
0	1	-
2	$\frac{1}{2}(3\cos^2\theta - 1)$	$\sqrt{\frac{3}{2}}\sin\theta\cos\theta$
4	$\frac{1}{8}(3 - 30\cos^2\theta + 35\cos^4\theta)$	$-\frac{\sqrt{5}}{4}\sin\theta\cos\theta(3 - \cos^2\theta)$

V. APPLICATIONS TO DIATOMIC MOLECULES N₂ AND O₂

A. Parallel Geometry, $\alpha = 0$: Elementary Expression of $T_e^{(n)}(\theta, \alpha = 0)$ for N₂

N₂ has σ_g symmetry, and we approximate its MO by the asymptotic approximation from single center molecule (Eq. (67)) with $m = 0$ and $l = 0, 2, 4$ [48, 49] whose angular coefficient are given in table II. The radial part of electronic wave function is given by

$$R_l(r) = r^{\eta-1} e^{-p_B r} \quad (104)$$

with $\eta \equiv Z_c/p_B$; Z_c is the core charge and $p_B = \sqrt{2|E_B|}$ with E_B is binding energy.

Evaluating Eq. (84) for $m = 0$ and $l_i, l_r = 0, 2, 4$ give us the HHG operator for N₂

$$T_e^{(n)}(\theta) = \sqrt{2\pi(n\omega)} \sum_{l_i, l_r=0,2,4} d_{00}^{l_r}(\theta) \tilde{a}_{zz}^n(l_r, l_i; 0) d_{00}^{l_i}(\theta) \quad (105)$$

Using the expressions for the reduced rotation matrices from Tab. I and simplifying, we may rewrite the operator as a sum of powers of $\cos^2 \theta$ only,

$$\begin{aligned}
T_e^{(n)}(\theta) &= \sqrt{2\pi(n\omega)} \left[b_0^{(n)} + b_1^{(n)} \cos^2 \theta + b_2^{(n)} \cos^4 \theta \right. \\
&\quad \left. + b_3^{(n)} \cos^6 \theta + b_4^{(n)} \cos^8 \theta \right] \quad (106)
\end{aligned}$$

where the coefficients $b_j^{(n)}$ s reads,

$$\begin{aligned}
b_0^{(n)} &= \tilde{a}_{zz}^{(n)}(0, 0; 0) - \frac{1}{2}\tilde{a}_{zz}^{(n)}(2, 2; 0) + \frac{3}{8}\tilde{a}_{zz}^{(n)}(4, 4; 0) \\
&\quad - \frac{1}{2}\left(\tilde{a}_{zz}^{(n)}(0, 2; 0) + \tilde{a}_{zz}^{(n)}(2, 0; 0)\right) \\
&\quad + \frac{3}{8}\left(\tilde{a}_{zz}^{(n)}(0, 4; 0) + \tilde{a}_{zz}^{(n)}(4, 0; 0)\right) \\
&\quad - \frac{3}{16}\left(\tilde{a}_{zz}^{(n)}(2, 4; 0) + \tilde{a}_{zz}^{(n)}(4, 2; 0)\right) \\
b_1^{(n)} &= -\frac{3}{2}\tilde{a}_{zz}^{(n)}(2, 2; 0) \\
&\quad + \frac{3}{2}\left(\tilde{a}_{zz}^{(n)}(0, 2; 0) + \tilde{a}_{zz}^{(n)}(2, 0; 0)\right) \\
&\quad - \frac{15}{4}\left(\tilde{a}_{zz}^{(n)}(0, 4; 0) + \tilde{a}_{zz}^{(n)}(4, 0; 0)\right) \\
&\quad - \frac{21}{16}\left(\tilde{a}_{zz}^{(n)}(2, 4; 0) + \tilde{a}_{zz}^{(n)}(4, 2; 0)\right) \\
b_2^{(n)} &= \frac{35}{8}\left(\tilde{a}_{zz}^{(n)}(0, 4; 0) + \tilde{a}_{zz}^{(n)}(4, 0; 0)\right) \\
&\quad - \frac{125}{16}\left(\tilde{a}_{zz}^{(n)}(2, 4; 0) + \tilde{a}_{zz}^{(n)}(4, 2; 0)\right) \\
b_3^{(n)} &= \frac{105}{16}\left(\tilde{a}_{zz}^{(n)}(2, 4; 0) + \tilde{a}_{zz}^{(n)}(4, 2; 0)\right) \\
b_4^{(n)} &= \frac{1225}{16}\tilde{a}_{zz}^{(n)}(4, 4; 0)
\end{aligned} \tag{107}$$

Thus, by using Eq. (62), the n th harmonic signal for N_2 becomes,

$$\begin{aligned}
S^{(n)}(t_d) &= \mathcal{C} \sum_{j=0}^3 \sum_{j' \geq j}^3 c_{jj'}^{(n)} \langle \langle \cos^{2j} \theta \rangle \rangle \langle \langle \cos^{2j'} \theta \rangle \rangle \\
&= \mathcal{C} \left\{ c_{00}^{(n)} + c_{01}^{(n)} \langle \langle \cos^2 \theta \rangle \rangle (t_d) \right. \\
&\quad + c_{11}^{(n)} \langle \langle \cos^2 \theta \rangle^2 \rangle (t_d) + c_{02}^{(n)} \langle \langle \cos^4 \theta \rangle \rangle (t_d) \\
&\quad \left. + \dots + c_{44}^{(n)} \langle \langle \cos^8 \theta \rangle^2 \rangle (t_d) \right\}
\end{aligned} \tag{108}$$

where $\mathcal{C} = (\sqrt{2\pi n\omega})^2 2\pi \frac{(n\omega)^2}{c^3} = (2\pi)^2 \left(\frac{n\omega}{c}\right)^3$. The coefficients $c_{jj'}^{(n)}$ are related to $b_j^{(n)}$ as follows

$$c_{j,j'}^{(n)} = \begin{cases} |b_j^{(n)}|^2 & \text{for } j = j' \\ 2Re\left(b_j^{(n)} b_{j'}^{(n)*}\right) & \text{for } j \neq j' \end{cases} \tag{109}$$

The leading two terms of the signal for N_2 , Eq. (108), consist of a constant term proportional to $c_{00}^{(n)}$, that arises from the leading angular momentum term $l = 0$ of the active molecular orbital of N_2 , and a term proportional to the second moment $\langle \langle \cos^2 \theta \rangle \rangle (t_d)$ that corresponds to the usual “degree of alignment” $A(t_d)$. We may note in passing that the above result does not support a recent model calculation [53, 54] that emphasizes that the leading contribution for HHG signal from N_2 arises from the fourth moment $\langle \cos^4 \theta \rangle$; that would require, for example, dropping the basic contribution of the $l = 0$ term i.e.

Table II: The molecular properties used in this work. I_p is adiabatic ionization potential, B is rotational constant of molecule, α_{\parallel} and α_{\perp} are parallel and perpendicular polarizability, and $C_l^{(m)}$'s are angular coefficient of the electronic wave function.

	N_2	O_2	Ref.
HOMO	$\sigma_g, m = 0$	$\pi_g, m = 1$	[22, 50]
I_p (eV)	15.58	12.03	[48]
B (cm^{-1})	2.0	1.4377	[51]
α_{\parallel} (\AA^3)	2.38	2.35	[52]
α_{\perp} (\AA^3)	1.45	1.21	[52]
$C_0^{(m)}$	2.02	-	[48]
$C_2^{(m)}$	0.78	0.62	[48]
$C_4^{(m)}$	0.04	0.03	[48]

$b_0^{(n)}$ in Eq. (106) – for the HHG operator for N_2 – that of course would not be justifiable due to the σ – *symmetry* of its active orbital.

B. Parallel Geometry, $\alpha = 0$: Elementary Expression of $T_e^{(n)}(\theta; \alpha = 0)$ for O_2

O_2 has π_g symmetry, and thus we approximate its MO by the asymptotic approximation with $m = 1$ and $l = 2, 4$ [48, 49] whose angular coefficient are given in table II. The HHG operator (Eq. (84)) for O_2 reads

$$\begin{aligned}
T_e^{(n)}(\theta) &= \sqrt{2\pi(n\omega)} \\
&\quad \times \sum_{l_i, l_r=2,4} d_{01}^{l_r}(\theta) \tilde{a}_{zz}^{(n)}(l_r, l_i; 1) d_{01}^{l_i}(\theta)
\end{aligned} \tag{110}$$

By using the expressions for the reduced rotation matrices from Tab. I and simplifying, we may rewrite the operator as a sum of powers of $\sin^2 \theta \cos^{2n} \theta$ only,

$$\begin{aligned}
T_e^{(n)}(\theta) &= \sqrt{2\pi(n\omega)} \left[b_1^{(n)} \sin^2 \theta \cos^2 \theta + b_2^{(n)} \sin^2 \theta \cos^4 \theta \right. \\
&\quad \left. + b_3^{(n)} \sin^2 \theta \cos^6 \theta \right]
\end{aligned} \tag{111}$$

where $b_j^{(n)}$ -coefficients are given by

$$\begin{aligned}
b_1^{(n)} &= \frac{3}{2}\tilde{a}_{zz}^{(n)}(2, 2; 1) + \frac{45}{16}\tilde{a}_{zz}^{(n)}(4, 4; 1) \\
&\quad - \frac{3}{4}\sqrt{\frac{15}{2}}\left(\tilde{a}_{zz}^{(n)}(2, 4; 1) + \tilde{a}_{zz}^{(n)}(4, 2; 1)\right) \\
b_2^{(n)} &= -\frac{105}{8}\tilde{a}_{zz}^{(n)}(4, 4; 1) \\
&\quad + \frac{7}{4}\sqrt{\frac{15}{2}}\left(\tilde{a}_{zz}^{(n)}(2, 4; 1) + \tilde{a}_{zz}^{(n)}(4, 2; 1)\right) \\
b_3^{(n)} &= \frac{245}{16}\tilde{a}_{zz}^{(n)}(4, 4; 1)
\end{aligned} \tag{112}$$

Finally, substituting operator expression (Eq. (111)) in Eq. (62) we obtain the n th signal of O_2 reads

$$\begin{aligned} S^{(n)}(t_d) &= \mathcal{C} \sum_{j=1}^3 \sum_{j' \geq j}^3 c_{jj'}^{(n)} \langle \langle \sin^2 \theta \cos^{2j} \theta \rangle \langle \sin^2 \theta \cos^{2j'} \theta \rangle \rangle \\ &= \mathcal{C} \left\{ c_{11}^{(n)} \langle \langle \sin^2 \theta \cos^2 \theta \rangle^2 \rangle (t_d) \right. \\ &\quad + c_{12}^{(n)} \langle \langle \sin^2 \theta \cos^2 \theta \rangle \langle \sin^2 \theta \cos^4 \theta \rangle \rangle (t_d) \\ &\quad \left. + \dots + c_{33}^{(n)} \langle \langle \sin^2 \theta \cos^6 \theta \rangle^2 \rangle (t_d) \right\} \quad (113) \end{aligned}$$

Above, coefficients $c_{jj'}^{(n)}$ are related to $b_j^{(n)}$ coefficients of Eq. (112) through Eq. (109).

We note that, unlike in the case of N_2 considered above, now there is no constant leading term in the signal for O_2 , Eq. (113). This is a consequence of the π -*symmetry* of the active orbital for O_2 , which does not permit the lowest $l = 0$ angular momentum component for its active orbital.

C. Arbitrary Relative Polarization Angle α : HHG Signal

We now consider the signals for N_2 and O_2 in the general case in which the probe and the pump polarizations make an arbitrary angle α between them, as shown in Fig. 3. Unlike alignment angle θ , the pump-probe angle α can be controlled in the laboratory and may provide a possible control of HHG of molecule. To obtain the signals in terms of elementary trigonometric functions in this more general case, we refer to Fig. 3. The direction of the molecular axis is now denoted by (θ', ϕ') . The same expression for the signal as in the parallel case now holds in terms of the primed angles. The HHG signal (Eq. (108) for N_2 and Eq. (113) for O_2) for arbitrary angle α now can be written as:

$$\begin{aligned} S^{(n)}(t_d; \alpha) &= \mathcal{C} \left\{ c_{00}^{(n)} + c_{01}^{(n)} \langle \langle \cos^2 \theta' \rangle \rangle (t_d) \right. \\ &\quad + c_{11}^{(n)} \langle \langle \cos^2 \theta' \rangle^2 \rangle (t_d) \\ &\quad \left. + \dots + c_{44}^{(n)} \langle \langle \cos^8 \theta' \rangle^2 \rangle (t_d) \right\} \quad (114) \end{aligned}$$

for N_2 and

$$\begin{aligned} S^{(n)}(t_d; \alpha) &= \mathcal{C} \left\{ c_{11}^{(n)} \langle \langle \sin^2 \theta' \cos^2 \theta' \rangle^2 \rangle (t_d) \right. \\ &\quad + c_{12}^{(n)} \langle \langle \sin^2 \theta' \cos^2 \theta' \rangle \langle \sin^2 \theta' \cos^4 \theta' \rangle \rangle (t_d) \\ &\quad \left. + \dots + c_{33}^{(n)} \langle \langle \sin^2 \theta' \cos^6 \theta' \rangle^2 \rangle (t_d) \right\} \quad (115) \end{aligned}$$

for O_2 . Above, $\langle \langle f(\theta') \rangle \rangle (t_d) = \sum_{J_0 M_0} \rho(J_0) \langle \Phi_{J_0 M_0}(t_d, \theta) | f(\theta') | \Phi_{J_0 M_0}(t_d, \theta) \rangle$ is an expectation value of function $f(\theta')$ given in probe frame but evaluated with respect to the rotational wave packet obtained in the pump frame. Before evaluating the

above integral, it is convenient, therefore, to transform the HHG operators in the variables (θ', ϕ') in the angles (θ, ϕ) of the pump-frame (i.e. with the z along the pump polarization). This can be done by the simple transformations, given by Eq. (92), where ϕ is the angle between plane of molecular axis - pump pulse and plane of pump - probe pulses. The elementary expression for the expectation value of the alignment operator $A(t_d; \alpha) = \langle \cos^2 \theta' \rangle$ in the case of non-zero angle α reads:

$$\begin{aligned} A(t_d; \alpha) &= \langle \cos^2 \theta' \rangle \\ &= \left(\cos^2 \alpha - \frac{1}{2} \sin^2 \alpha \right) \langle \cos^2 \theta \rangle + \frac{1}{2} \sin^2 \alpha \\ &\quad + \frac{1}{4} \sin^2 \alpha (\langle \sin^2 \theta e^{2i\phi} \rangle + c.c.) \\ &\quad + \frac{1}{2} \sin 2\alpha (\langle \sin \theta \cos \theta e^{i\phi} \rangle + c.c.) \quad (116) \end{aligned}$$

where $\langle \sin \theta \cos \theta e^{\pm i\phi} \rangle$ couples the J' states with $\Delta J = 0, \pm 2$ and $\Delta M = \pm 1$ whereas $\langle \sin^2 \theta e^{\pm 2i\phi} \rangle$ couples the J' states with $\Delta J = 0, \pm 2$ and $\Delta M = \pm 2$. We note that for the linearly polarized pump pulse of the present interest, the interaction Hamiltonian is proportional to $\cos^2 \theta$, which is independent of M in the space fixed pump-frame. Thus the M -quantum number of the rotational wave-packet remains constant, or $M = M_0$, throughout the evolution. Hence, the expectation values of $\langle \sin \theta \cos \theta e^{\pm i\phi} \rangle$ and $\langle \sin^2 \theta e^{\pm 2i\phi} \rangle$ vanish and we get,

$$\langle \cos^2 \theta' \rangle = \frac{1}{2} (3 \cos^2 \alpha - 1) \langle \cos^2 \theta \rangle + \frac{1}{2} \sin^2 \alpha \quad (117)$$

In a similar way, we obtain the expectation value for higher order

$$\begin{aligned} \langle \cos^4 \theta' \rangle &= \frac{1}{8} (35 \cos^4 \alpha - 30 \cos^2 \alpha + 3) \langle \cos^4 \theta \rangle \\ &\quad + \frac{3}{8} (-10 \cos^4 \alpha + 12 \cos^2 \alpha - 2) \langle \cos^2 \theta \rangle \\ &\quad + \frac{3}{8} \sin^4 \alpha \quad (118) \end{aligned}$$

We note in passing that for $\alpha = 0$, $\langle \cos^2 \theta' \rangle$ in Eq. (117) and $\langle \cos^4 \theta' \rangle$ in Eq. (118) reduce to $\langle \cos^2 \theta \rangle$ and $\langle \cos^4 \theta \rangle$, respectively.

Thermal averaging Eq. (117) gives us the “degree of alignment” or the alignment-moment:

$$A(t_d, \alpha) = \frac{1}{2} (3 \cos^2 \alpha - 1) \langle \langle \cos^2 \theta \rangle \rangle (t_d) + \frac{1}{2} \sin^2 \alpha \quad (119)$$

which also appears in the second leading term of the signal for N_2 , for arbitrary angle α , (see, Eq. (114)). Squaring and taking the thermal average of Eq. (117) gives us $\langle \langle \cos^2 \theta' \rangle^2 \rangle$, which is the third term of HHG signal of N_2 . The thermal average of Eq. (118) gives us $\langle \langle \cos^4 \theta' \rangle \rangle$

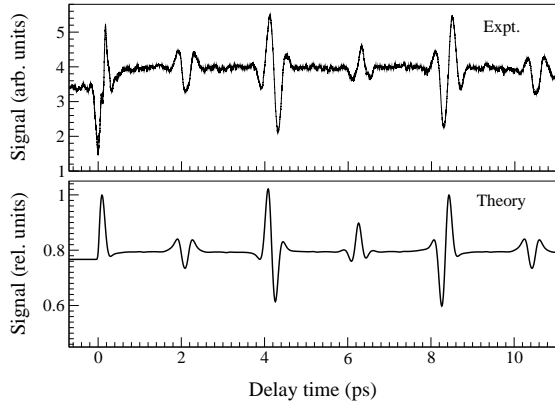


Figure 4: Comparison of the experimental [13, 55] and the theoretical dynamic 19th HHG signal for N_2 ; pump intensity $I = 0.8 \times 10^{14} \text{ W/cm}^2$, probe intensity $I = 1.7 \times 10^{14} \text{ W/cm}^2$; duration 40 fs, wavelength 800 nm, temperature 200 K.

which appears in the fourth term of HHG signal of N_2 . The difference of Eq. (117) and Eq. (118) gives us

$$\begin{aligned} \langle \sin^2 \theta' \cos^2 \theta' \rangle = & \frac{1}{8} (-35 \cos^4 \alpha + 30 \cos^2 \alpha - 3) \langle \cos^4 \theta \rangle \\ & + \frac{1}{8} (30 \cos^4 \alpha - 24 \cos^2 \alpha + 2) \langle \cos^2 \theta \rangle \\ & + \frac{1}{8} (-3 \sin^4 \alpha + 4 \sin^2 \alpha) \end{aligned} \quad (120)$$

Squaring and then thermally averaging Eq. (120) yields the leading term of HHG signal of O_2 , given by Eq. (115). In a similar way, we can explicitly exhibit the α -dependence of the higher order terms in the signal for O_2 , Eq. (115), as well.

VI. RESULTS AND DISCUSSIONS

A. Signals in the Time Domain

We now apply the theory to analyze the observed HHG signals from the diatomic molecules, N_2 and O_2 . In typical recent experiments (e.g. [11, 12, 13, 55]) an ensemble of N_2 or O_2 molecules is first set into free rotation by a femtosecond pump pulse. The HHG signals were detected by monitoring the emission due to a second more intense femtosecond probe pulse, that was delayed with respect to the first by successively increasing the time intervals, t_d , in the picosecond domain, between them.

In the experiments for N_2 , for example by Miyazaki et al. [13, 55], a peak pump-intensity $I_1 = 0.8 \times 10^{14} \text{ W/cm}^2$, a peak probe-intensity $I_2 = 1.7 \times 10^{14} \text{ W/cm}^2$ were used; the central wavelength $\lambda = 800 \text{ nm}$ and the pulse duration $\tau = 40 \text{ fs}$ were kept the same for both the pulses. For the experiment with O_2 , the harmonic signal was measured in a similar fashion for $I_1 = 0.5 \times 10^{14} \text{ W/cm}^2$ and $I_2 = 1.2 \times 10^{14} \text{ W/cm}^2$; the other parameters were kept the same as in the case

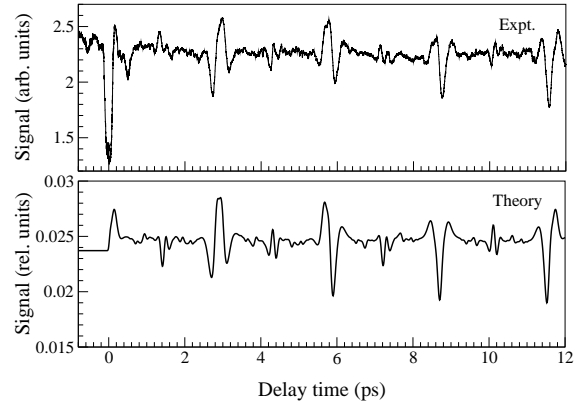


Figure 5: Comparison of the experimental [13, 55] and the theoretical 19th harmonic dynamic signal for O_2 ; pump intensity $I = 0.5 \times 10^{14} \text{ W/cm}^2$, probe intensity $I = 1.2 \times 10^{14} \text{ W/cm}^2$; durations 40 fs, wavelengths 800 nm, temperature 200 K.

of N_2 . For the purpose of a direct comparison, our calculations were performed for the same parameter values as in these experiments [13, 55]. In Fig. 4 and Fig. 5, we compare the calculated HHG signals as a function of t_d for N_2 and O_2 , with the experimental data obtained for the 19th order harmonic. The effective ensemble temperature was taken to be $T = 200 \text{ K}$, that was estimated from the matching of the peak position of the spectral distribution with that of the Boltzmann distribution as suggested first in [19]. It can be seen from Fig. 4 that the experimental data for N_2 show the “revival” phenomenon with a full revival period $T_{rev} = 8.4 \text{ ps}$ (which is consistent with the rotational constant of N_2 (cf. Tab. II)) as well as a $\frac{1}{2}$ and a $\frac{1}{4}$ fractional-revival. The observed signal for O_2 shows, in addition to the full revival (period for O_2 is $T_{rev} = 11.6 \text{ ps}$) and two fractional revivals similar to the two seen for N_2 , an additional $\frac{1}{8}$ revival. The calculated signals can be seen to follow the same sequence of the full and the three fractional revivals as seen in the experimental signal. We note that these observations for N_2 and O_2 are also consistent with the data of Itatani et al. [11] and Kanai et al. [12].

To understand the similarities and the differences between the signals for N_2 and O_2 , we use the analytical results of the present theory below. The properties of the HHG signal of N_2 are governed by Eq. (108). The first term gives a constant background. The second term $\langle \langle \cos^2 \theta \rangle \rangle(t_d)$ is the dominant dynamic term and makes the signal to mimic the “degree of alignment” $A(t_d) \equiv \langle \langle \cos^2 \theta \rangle \rangle(t_d)$. The third term $\langle \langle \cos^2 \theta \rangle^2 \rangle(t_d)$ give unequal maxima and minima i.e. the difference between the maximum signal and the average signal is greater than the difference between the average signal and the minimum signal. Furthermore we point out that at a lower initial temperature, the valley of $\langle \langle \cos^2 \theta \rangle^2 \rangle(t_d)$ that occurs, for higher temperatures, at the $\frac{1}{4} T_{rev}$ revival, can *split* into two valleys, due to

this term, and thus the third term can strongly affect the HHG spectrum, as can be seen in the experiment by Itatani, *et al.* [11, 14]. Another earlier puzzle regarding its dynamic signal observed was the failure of the alignment measure $A(t_d) = \langle \langle \cos^2 \theta \rangle \rangle (t_d)$ to account for the dynamic HHG signal for O_2 , observed by Itatani *et al.* [11]. In fact, Itatani *et al.* found that their data behaved more closely to the expectation value $B(t_d) \equiv \langle \langle \sin^2 2\theta \rangle \rangle (t_d)$. From Eq. (113) it can be seen that indeed the *leading* term of the signal for O_2 is given by $\langle \langle \sin^2 \theta \cos^2 \theta \rangle \rangle (t_d) = \frac{1}{16} \langle \langle \sin^2 2\theta \rangle \rangle (t_d)$, which is directly proportional to the observed signal. Moreover, the present theory also predicts that there ought to be modifications to this result due to the higher order terms in Eq. (113). In contrast to N_2 there is no significant difference between minima and maxima for O_2 , since all terms in Eq. (73) have similar minima and maxima. The present theory also predicts that there ought to be modifications to this result due to the higher order terms in Eq. (113). In contrast to N_2 , however, there should not be a significant asymmetry between the size of the maxima and the minima for O_2 , since the terms in Eq. (73) have similar maxima and minima. This can be, however, quantitative contributions from the higher order terms predicted by the theory. In fact, as mentioned earlier, Kanai *et al.* [12] found empirically that their experimental HHG signals for N_2 and O_2 demanded heuristic introduction of operators involving *higher* orders of $\cos^2 \theta$ functions, or Legendre polynomials, as the dynamic signal could not be well expressed in term of $\langle \langle \cos^2 \theta \rangle \rangle (t_d)$ only for N_2 , or $\langle \langle \sin^2 2\theta \rangle \rangle (t_d)$ only for O_2 . In fact, the present theory provides an *ab initio* derivation of the desired general expansion of the HHG signal in terms of the moments of the Legendre polynomials Eq. (103) and/or of the powers of $\cos^2 \theta$, e.g. Eqs. (113) and (108).

A related characteristic of interest first observed by Miyazaki *et al.* (e.g. [55]) is the appearance of extra series and lines in the Fourier spectrum of the dynamic HHG signal for *both* N_2 and O_2 , that are Raman forbidden. These extra lines can not be attributed to $A(t_d) = \langle \langle \cos^2 \theta \rangle \rangle (t_d)$, for N_2 , or to $B(t_d) = \langle \langle \sin^2 2\theta \rangle \rangle (t_d)$ for O_2 . It will be seen below that the *F.T.* of the higher order terms of Eq. (108) for N_2 and of Eq. (113) for O_2 , given by the present theory can consistently account for their appearance.

Comparing the expressions for the signals for N_2 and O_2 and directly calculating the $c_{jj'}^{(n)}$ coefficients in the respective signals it is found that the signal for N_2 is much stronger than that for O_2 , as also observed experimentally [55].

We may briefly discuss here the dependency of the HHG signals on the initial temperature, an example of which is shown in Fig. 6. It can be seen from the figure that the lower initial temperature gives a greater amplitude of revival. This may be understood as follows. A lower initial temperature gives a lower value of the maximum of the statistically occupied J_0 levels and hence

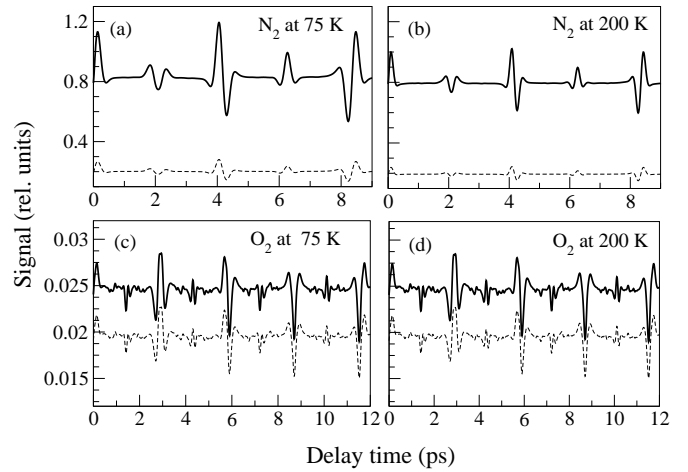


Figure 6: The dependency of HHG signal on the harmonic order and on the initial temperature of the gas. Solid and dashed lines are for the 19th and the 21th order, respectively.

also a lower value of the maximum initial value of M_0 , than at a higher temperature. As a result of interaction with the linearly polarized pump pulse (quantization axis along the polarization axis) at a given intensity, each wavepacket that evolves from a given initial $|J_0 M_0\rangle$ state, can couple to the higher levels $J' > \max(J_0)$ but can not raise the initial maximum value of M_0 . Therefore, for a given intensity, the ratio of J' to M_0 is higher for a lower temperature, and as a consequence the degree of alignment $A(t_d) = \langle \langle \cos^2 \theta \rangle \rangle$ tends to be also higher, implying that the molecule becomes more strongly aligned during a revival.

B. Rotational Revivals: Periods and Phases

If a linear molecule has a permanent dipole moment (e.g. hetero-nuclear diatomics), then the interaction Hamiltonian of the (pump) laser with the molecular frame depends on the first power of $\cos \theta$, where θ is the angle of rotation of the molecular axis with respect to the laser polarization axis. In contrast, the interaction with the polarizability of the molecule (e.g. for homo- or hetero-nuclear diatomics) depends on $\cos^2 \theta$. Thus in general the interaction may contain the operators $\cos^n \theta$ with $n = 1$ and/or 2. Then in either case, the rotational wavepackets created by the laser can be written in the form:

$$\begin{aligned} \Phi_{J_0 M_0}(t) = & \sum_{j=0,1,2,3,\dots} C_{J_0+nj, M_0}(t) \\ & \times e^{-\frac{i}{\hbar} E_{J_0+nj} t} |J_0 + nj, M_0\rangle \end{aligned} \quad (121)$$

This can be obtained, for example, from a consideration of the perturbative solution of Eq. (39) in successive power of the interaction Hamiltonian, and noting

that the rotational eigenstates couple either by $P_2(\cos \theta)$ (in the absence of a permanent dipole moment) with a minimum (non-zero) $n = 2$ or by $P_1(\cos \theta)$ and $P_2(\cos \theta)$ (in the presence of a permanent dipole moment) with a minimum $n = 1$. It can be readily understood from the well known properties of the vector addition coefficients that appear in the integration over the product of three spherical harmonics (cf. para below) that the expectation value of the N th cosine-moment with respect to a rotational wavepacket at a time $t = t_d$, takes the form:

$$\begin{aligned}
\langle \cos^N \theta \rangle_{J_0 M_0}(t_d) &= \langle \Phi_{J_0 M_0}(t_d) | \cos^N \theta | \Phi_{J_0 M_0}(t_d) \rangle \\
&= \sum_s \sum_{p=-s}^s \sum_{j=0,1,2,3,\dots}^N \\
&\times C_{J_0+nj+p, M_0}^{J_0 M_0*}(t_d) C_{J_0+nj, M_0}^{J_0 M_0}(t_d) \\
&\times a_s \langle Y_{J_0+nj+p, M_0} | Y_{s,0} | Y_{J_0+nj, M_0} \rangle \\
&\times \exp \left(-\frac{i}{\hbar} (E_{J_0+nj+p} - E_{J_0+nj}) t_d \right)
\end{aligned} \tag{122}$$

where, the integers s and p have the same parity (even or odd) as the parity of N . This follows from the fact that $\cos^N \theta$ can be expressed as a linear combination: $\cos^N \theta = \sum_s a_s P_s(\cos \theta)$, for all s up to N , and since the matrix elements $\langle Y_{J_0+nj', M_0} | Y_{s,0} | Y_{J_0+nj, M_0} \rangle = 0$, unless, $J_0 + nj' = J_0 + nj + (p - s) \geq 0$, and $J_0 + nj + (p - s) + J_0 + nj + s = \text{even}$. Thus, the phase of each individual term of Eq. (122), for any given value of the integers J_0, n, N, j , is given by

$$\begin{aligned}
\Delta \phi_{n,N}^{J_0}(t_d) &= \frac{1}{\hbar} (E_{J_0+nj+p} - E_{J_0+nj}) t_d \\
&\times 2\pi \hbar B c t (\pm 2pJ_0 \pm 2npj + p^2 \pm p) \\
&= 2\pi \frac{t_d (\hbar B c) 2}{\hbar} \left(J_0 + nj + \frac{p^2 + p}{2} \right) \tag{123}
\end{aligned}$$

where, we have used $E_{J,M} \equiv J(J+1)\hbar Bc$; B is the rotational constant, $T_{rev} \equiv \frac{1}{2Bc}$ is the rotational period, and $\hbar = 2\pi\hbar$. We note first that the quantity in the last parentheses above is an integer, independent of the value of j and J_0 . We note that the maximum value of s or p above is N . The phase difference (Eq. (123)) therefore equals to an even or odd multiple of π , or odd multiple of $\frac{\pi}{2}$, depending on the parity of the groups of rotational states. Therefore, the shortest time period for which the phases of *all* terms or all terms within a parity group become equal in Eq. (123), and hence coherently enhance the signal, is clearly

$$T_{min} = \frac{1}{nN} T_r. \tag{124}$$

For times between the successive coherent enhancements or “revivals”, the individual phases in Eq. (123) disperse away from one another and the revival peaks tend to

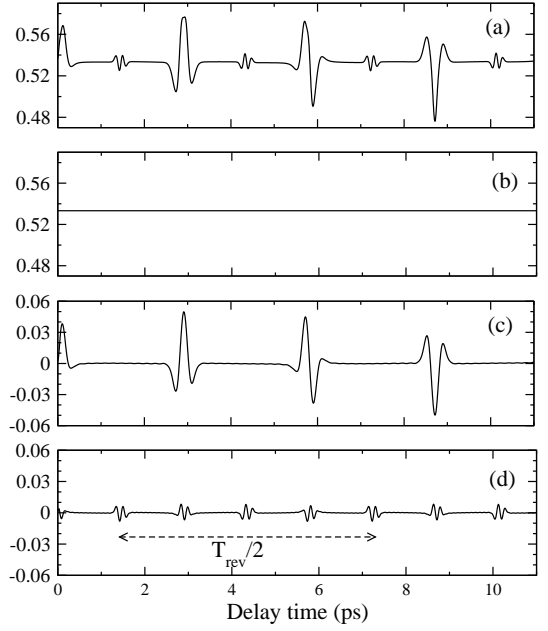


Figure 7: Revival structure of the moment $\langle \langle \sin^2 2\theta \rangle \rangle(t_d)$, for the case of O₂, on the beat frequency: for all ΔJ retained (panel a), with $\Delta J = 0$ only (panel b), with $\Delta J = \pm 2$ only (panel c), and with $\Delta J = \pm 4$ only (panel d). It is clear that the transition with $\Delta J = \pm 4$ has the lowest fractional revival at $\frac{1}{8}T_{rev}$, and has the shortest period.

be washed out by destructive interference, and the HHG signal reduces to the average or the back-ground level.

We may summarize the above result as a “revival theorem”: If the laser-molecule interaction Hamiltonian is characterized by the lowest power n of $\cos^n \theta$, with $n = 1$ or 2 , θ is the rotation angle, and if the highest discernible (numerically significant) moment in the expression of the signal is $\langle \Phi_{J_0 M_0}(t) | \cos^N \theta | \Phi_{J_0 M_0}(t) \rangle$, $N \geq 1$, then the experimental signal would exhibit as many as $n \times N$ revivals within a full period $T_r = \frac{1}{2Bc}$, B is the rotational constant. Inversely, by counting the number of fractional revivals in the observed HHG signal, one may determine the highest order, N , and hence also the significant “cosine moments” (up to the order N) that would be necessary to fit the observed signal. We may note that the above theorem covers the well-known cases of fractional revivals discussed earlier [56, 57, 58, 59] as special cases.

For homonuclear diatomic molecules with no permanent dipole moment, the lowest order pump pulse interaction is due to the polarizability tensor with $n = 2$. Thus for the standard alignment moment, $A(t_d) \equiv \langle \langle \cos^2 \theta \rangle \rangle(t_d)$ with $N = 2$, we get the lowest fractional period $T_{\frac{1}{4}} = \frac{1}{4}T_r$, and the subsequent two fractional revivals $T_{\frac{3}{4}}, T_{\frac{5}{4}}$ (defined analogously) and the full revival at T_r , with in a period. Thus the presence of the highest significant fourth cosine-moment with $N = 4$ would show the lowest $\frac{1}{nN} = \frac{1}{8}$ revival, plus the subsequent six fractional revivals at $(\frac{1}{4}, \frac{3}{8}, \frac{1}{2}, \frac{5}{8}, \frac{3}{4}, \frac{7}{8}) T_r$, within a

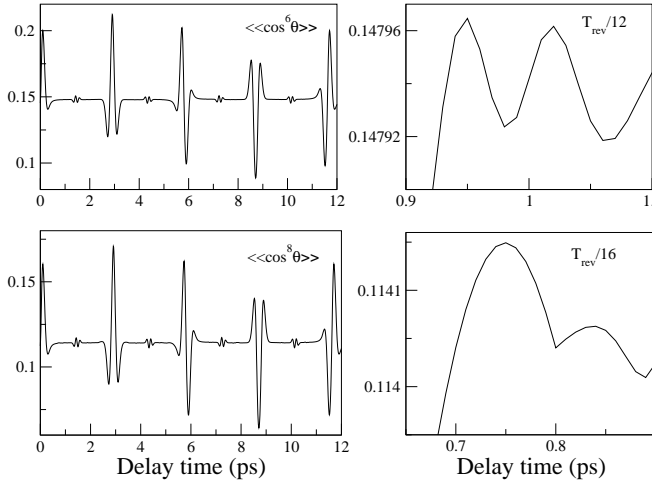


Figure 8: Weak components of the fractional revivals in the dynamical alignment signal for the case of O_2 . Contribution from $\langle\langle\cos^6\theta\rangle\rangle(t_d)$, near $T_{rev}/12$ (upper panel), and from $\langle\langle\cos^8\theta\rangle\rangle(t_d)$, near $T_{rev}/16$ (lower panel). They can hardly be detected in the full delay-time signal that is dominated by the leading lower order moments. $I = 0.5 \times 10^{14}$ W/cm 2 , FWHM 40 fs, and initial temperature 300 K.

full period T_r . An example containing the effect of the fourth cosine-moment is $B(t_d) = \langle\langle\sin^2 2\theta\rangle\rangle(t_d)$, which is illustrated in Fig. 7. For a heteromolecular diatomic molecule with a permanent dipole moment, the lowest order interaction Hamiltonian is characterized by the first power of $\cos\theta$ i.e. $n = 1$. Thus the alignment measure, a cosine moment with $N = 2$, will show $n \times N = 2$ revivals within in the full period. Higher order revivals may occur since Eq. (124) in principle holds for any combination (N, n) . We may recall, however, that for large N , the expectation value might be too weak for the lowest fractional revivals to be measured with sufficient resolution in practice. This circumstance is illustrated in Fig. 8 which shows the high order fractional revivals for $N = 6$ and $N = 8$ cosine-moments, $\langle\langle\cos^6\theta\rangle\rangle(t_d)$ and $\langle\langle\cos^8\theta\rangle\rangle(t_d)$, along with their magnifications.

C. Phase Relations of Fractional Revivals

Can one predict the relative phases of the fractional revivals? We may answer this question positively. From the phase difference (Eq.(123)), one finds:

$$\begin{aligned} \Delta\phi_{2,2}^{J_0+1}(T_{rev}) - \Delta\phi_{2,2}^{J_0}(T_{rev}) &= 4\pi \\ \Delta\phi_{2,2}^{J_0+1}(T_{rev}/2) - \Delta\phi_{2,2}^{J_0}(T_{rev}/2) &= 2\pi \\ \Delta\phi_{2,2}^{J_0+1}(T_{rev}/4) - \Delta\phi_{2,2}^{J_0}(T_{rev}/4) &= \pi \end{aligned} \quad (125)$$

Eq. (125) predicts that at $\frac{1}{4}T_r$ the phase for J_{even} is an exact mirror image of the phase for J_{odd} , as in fact is the case in Fig. 9, calculated for N_2 . From the above, we may further predict that:

(a) for O_2 , which posses J_{odd} levels only, will show a

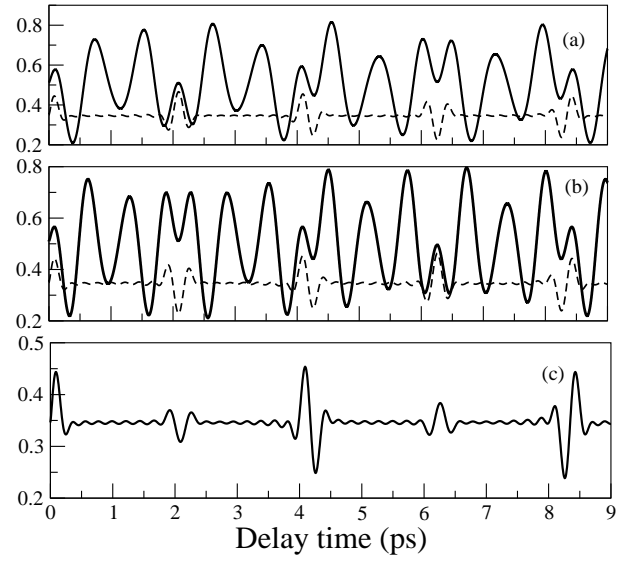


Figure 9: Dependence of alignment moment $\langle\langle\cos^2\theta\rangle\rangle(t_d)$ (for the case of N_2) on $|J_0, M_0\rangle$. Panel (a): calculated with a single state $|5, 0\rangle$ only (solid line), and retaining all odd J_0 with $J_{max} = 19$ (dashed line). Panel (b): with $|6, 0\rangle$ only (solid line), and all even J_0 with $J_{max} = 20$ (dashed line). Panel (c): calculated with all J upto $J_{max} = 20$. Results are for pulse intensity 0.8×10^{14} W/cm 2 and with FWHM 40 fs, for initial temperature 300 K.

“peak” at $T_r/4$,

(b) CO_2 , which possesses J_{even} levels only, will show a “valley” at $T_r/4$, and

(c) N_2 , which possesses both the majority J_{even} levels and the minority J_{odd} levels in the ratio 2 : 1 (due to the nuclear statistics of the molecule [22]), will show the revival at $T_r/4$ that would be a “valley” like the one for the J_{even} levels only, but with only half its normal “depth”, due to the counter contribution from the minority J_{odd} levels.

We note that one may also predict the nuclear statistics of such molecules by comparing the revival shape at $T_{rev}/2$ and $T_{rev}/4$. Let us first define a modulation amplitude at half-revival to be equal to the difference between peak and the base (or average) signal: $(A_{1/2} = S_{1/2}^{top} - S_{1/2}^{av.})$. Similarly, a modulation amplitude at quarter revival is equal to the difference between the top and the base (average) signal: $(A_{1/4} = S_{1/4}^{top} - S_{1/4}^{av.})$. The amplitude at half-revival is a sum of even and odd J contributions, and therefore $A_{1/2}$ is always positive. In contrast, the amplitude at the quarter-revival arises from their difference, and therefore $A_{1/4}$ can be positive (if it makes a “top” alignment) or negative (if it makes an “anti-top” alignment). Therefore, the existence of a “top” signal at the quarter-revival is a sign that even J levels are dominant. Similarly the presence of an “anti-top” signal at the quarter-revival signal is a sign of dominant odd J levels. From this observation, one can deduce the nuclear statistics from the ratio between the effective

(finite) number of even and the odd J levels (J_{even} and J_{odd} , respectively) excited:

$$\frac{J_{even}}{J_{odd}} = \frac{A_{1/2} - A_{1/4}}{A_{1/2} + A_{1/4}} \quad (126)$$

Thus, for example, the dynamic signal of O_2 shows $A_{1/2} = A_{1/4}$ indicating the absence of the even J levels. In contrast, $A_{1/2} = -A_{1/4}$ for CO_2 , indicating the absence odd J levels. For N_2 , we have $A_{1/4} = -\frac{1}{3}A_{1/2}$, and hence we have $J_{even} : J_{odd} = 2 : 1$. This property might be used for detecting the existence of isotopes of a molecular sample, as has been suggested recently [60].

D. Beat Frequencies

From Eq. (122), it is seen that the phase difference associated with $\langle \cos^2 \theta \rangle$ is $(B/\hbar)(4J+6)$. For B in cm^{-1} , the phase difference reads

$$\Delta\phi(J \rightarrow J \pm 2) = 2\pi Bc(4J+6) \quad (127)$$

with c in $cm/second$. According to Eq. (127), one can make a Fourier transform of $\langle \cos^2 \theta \rangle$ using Bc as basis frequency and find a series of peaks at $(4J+6)$. Fig. 10 shows the Fourier transform of $\langle \cos^2 \theta \rangle$ of N_2 , O_2 , and CO_2 . The spectrum of O_2 has peak series at $(10, 18, 26, \dots)Bc = (4J_{odd} + 6)Bc$, showing that O_2 has odd J levels only. In contrast, the peak series of CO_2 are located at $(6, 14, 22, 30, \dots)Bc = (4J_{even} + 6)$, showing that CO_2 has even J levels only. For N_2 , we obtain a series $(6, 14, 22, 30, \dots)Bc = (4J_{even} + 6)$ that is twice as strong as the series $(10, 18, 26, \dots)Bc = (4J_{odd} + 6)$. It implies that both even and odd J levels are present in N_2 , in the ratio $J_{even} : J_{odd} = 2 : 1$. These conclusions are consistent with the analysis based on the dynamic signals.

For $\langle \sin^2 2\theta \rangle$, there are two kinds of difference beat frequency. The first one is related to the transition with $\Delta J = \pm 2$ and is expressed by Eq. (127). The second one is related to the transitions with $\Delta J = \pm 4$ and can be expressed as

$$\Delta\phi(J \rightarrow J \pm 4) = 2\pi Bc(8J+20) \quad (128)$$

As a result, in addition to the series of lines $(4J+6)$, the Fourier transform of $\langle \sin^2 2\theta \rangle$ also has another series of lines at $(8J+20)$, with $\Delta J = 4$. Fig. 11 shows the calculated Fourier transform of $\langle \sin^2 2\theta \rangle$ of O_2 . It is seen from Fig. 11, that the first series ($\Delta J = \pm 2$) reaches its maximum at $J_{max} = 11$, while the second one ($\Delta J = \pm 4$) at $J_{max} = 13$. This difference comes from the fact that the $\Delta J = 4$ transition requires $\Delta J = 2$ as an intermediate transition. As a result, a $\Delta J = 4$ transition can occur one step after the $\Delta J = 2$ transition; for O_2 with only J_{odd} levels present, this implies a shift in J by 2, from $J_{max} = 11$ to $J_{max} = 13$, as seen above. From Fig. 11 one also finds that the intensity of the second transition is smaller than of the first one. This arises

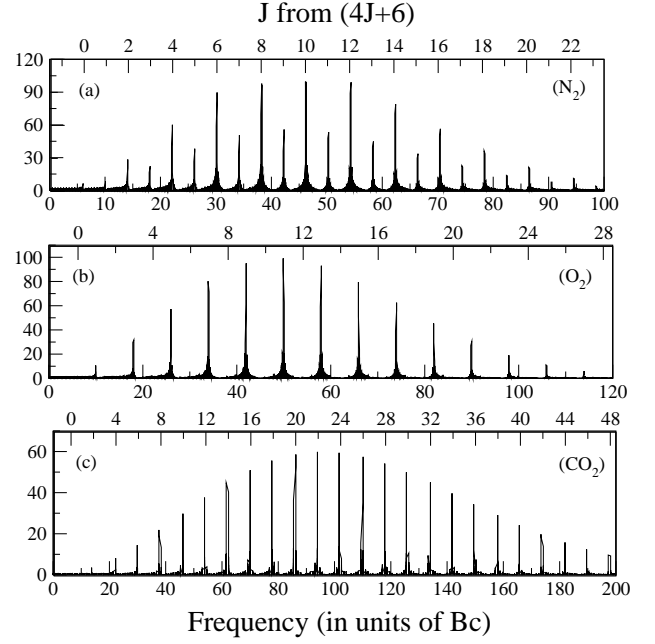


Figure 10: Fourier transform of the alignment moment $A(t_d) \equiv \langle \langle \cos^2 \theta \rangle \rangle(t_d)$, plotted using Bc as the basis frequency (lower scale). Following the $(4J+6)$ -rule for the line positions from $\langle \langle \cos^2 \theta \rangle \rangle$, the peak frequencies are seen to occur for odd J only, for the case of O_2 , even J only for the case of CO_2 , and for both even and odd J , for the case of N_2 . The corresponding J values are shown in upper scale.

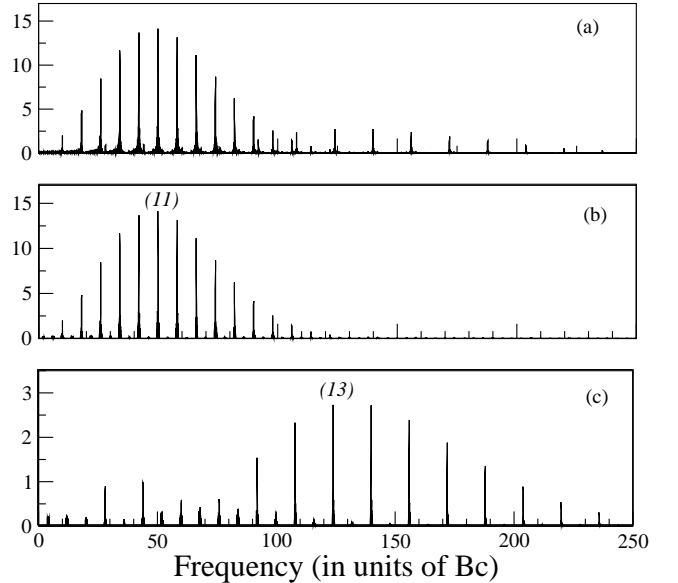


Figure 11: Fourier transform of $\langle \langle \sin^2 2\theta \rangle \rangle$ of O_2 : all lines (panel a), line from transitions with $\Delta J = \pm 2$ only (panel b), and lines from transition with $\Delta J = \pm 4$ only (panel c); pulse of intensity $0.5 \times 10^{14} W/cm^2$, FWHM = 40 fs, initial temperature 300 K.

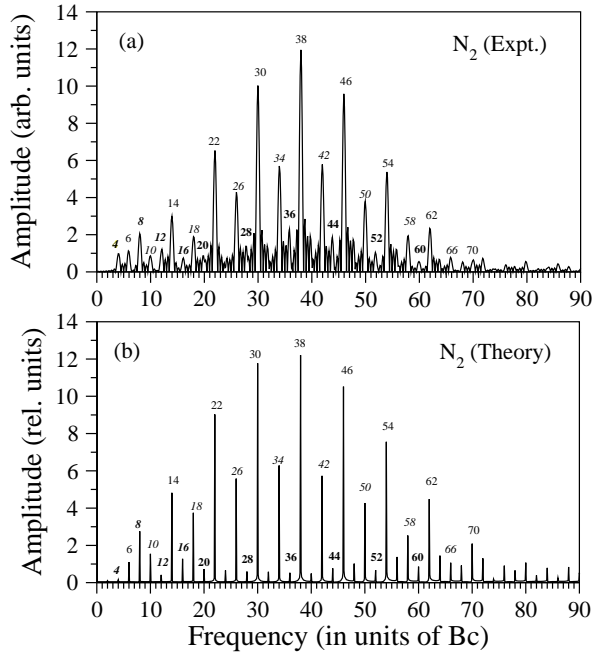


Figure 12: Comparison of the experimental [13] vs. the theoretical Fourier spectrum for the dynamic 19th harmonic signal for N_2 (Fig. 4). Both spectra show: series I: (6, 14, 22, 30, 38, ...) Bc , series II: (10, 18, 26, 34, 42, ...) Bc , series III: (20, 28, 36, 44, 52, 60, ...) Bc , and series IV: (4, 8, 12, 16, ...) Bc .

from the circumstance that the allowed matrix element of the second transition with the greater separation in J is weaker than the one with the lesser separation.

E. Signals in the Frequency Domain

To further compare with experimental data, we Fourier transform the calculated dynamic signals to get their spectra in the frequency domain. They may then be compared with the $F.T.$ of the experimental data. The results for the 19th harmonic signal for N_2 is compared with the experimental data in Fig. 12. It can be seen that the experimental spectrum (panel a) exhibits two prominent series I: (6, 14, 22, 30, ...) Bc and II: (10, 18, 26, 34, ...) Bc , which are also present in the theoretical spectrum (panel b). They can be easily understood to arise from the $F.T.$ of the $\langle\langle\cos^2\theta\rangle\rangle(t_d)$ term in Eq. (108) which vanishes unless $\Delta J = 0, \pm 2$; this produces a sequence of lines $(E_{J+2} - E_J)/2\pi = (4J + 6) Bc$, and gives the series I and II, for the even and the odd J levels, respectively. The relative prominence of the series I over the series II, from both experiment and theory, seen in the two panels in Fig. 12, could be understood as the 2 : 1 ratio of the J even over J odd levels, a well-known consequence of the nuclear spin statistics of N_2 (e.g. [8, 22]). The weakly resolved series III: (20, 28, 36, 44, ...) Bc and series IV: (4, 8, 12, 16, ...) Bc in Fig. 12(a) are the un-

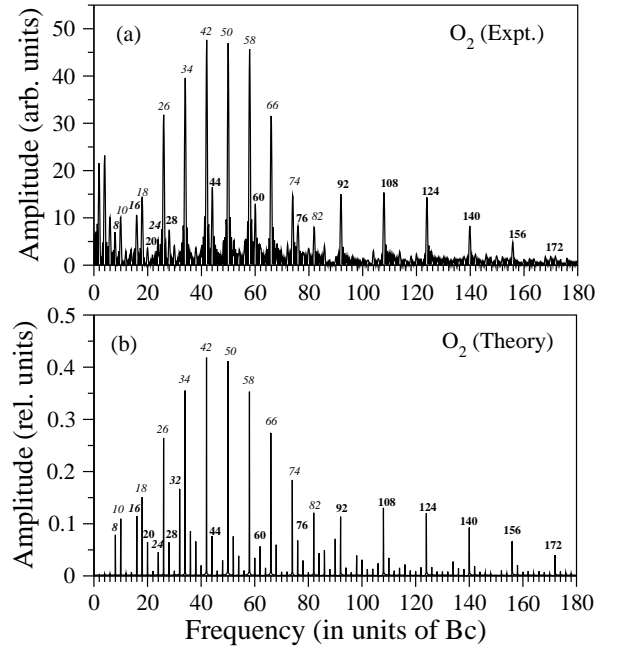


Figure 13: Comparison of the experimental [13] vs. theoretical Fourier spectrum of the dynamic 19th harmonic signal for O_2 (Fig. 5). Both the spectra show: series II: (10, 18, 26, 34, 42, ...) Bc , series III: (20, 28, 36, 44, 52, 60, ...) Bc , and series V: (8, 16, 24, ...) Bc .

expected series that could not be produced by the $F.T.$ of the leading term $\langle\langle\cos^2\theta\rangle\rangle(t_d)$. We note that the series III and IV, although weak, are certainly also present in the theoretical spectrum in Fig. 12(b). To interpret their origin, we consider the two higher order terms involving $\langle\langle\cos^2\theta\rangle^2\rangle(t_d)$ and $\langle\langle\cos^4\theta\rangle\rangle(t_d)$ in the signal for N_2 , Eq. (108). Because of the presence of the square of the second moment, the expected beat frequency from $\langle\langle\cos^2\theta\rangle^2\rangle(t_d)$ not only includes the frequencies $(4J + 6)Bc$ but also their sum and difference frequencies, as indicated below:

$$\begin{aligned}
& (a + b \cos \omega_1 t) (a' + b' \cos \omega'_1 t) \\
&= aa' + a'b \cos \omega_1 t + ab' \cos \omega'_1 t + bb' \cos \omega_1 t \cos \omega'_1 t \\
&= aa' + a'b \cos \omega_1 t + ab' \cos \omega'_1 t \\
&\quad + \frac{bb'}{2} \cos(\omega_1 + \omega'_1) t + \frac{bb'}{2} \cos(\omega_1 - \omega'_1) t \quad (129)
\end{aligned}$$

Above, the term a arises from transition with $\Delta J = 0$ with $\omega_0 = 0$. The frequency ω_1 arises from transition with $\Delta J = \pm 2$. The sum frequency $(\omega_1 + \omega'_1)$ yields $(E_{J+2} - E_J)/2\pi \equiv (4(J + J') + 12) Bc$ series whereas the difference $(\omega_1 - \omega'_1)$ produces $(E_{J+2} - E_J)/2\pi \equiv (4(J - J') Bc) > 0$. For integer J and J' they yield the series IV: (4, 8, 12, 16, ...) Bc . The next term $\langle\langle\cos^4\theta\rangle\rangle(t_d)$ vanishes unless $\Delta J = 0, \pm 2$, and ± 4 produces not only $(E_{J+2} - E_J)/2\pi = (4J + 6) Bc$ sequences lines but also $(E_{J+4} - E_J)/2\pi = (8J + 20) Bc$

Table III: List of all the predicted series arising from the moments $\langle\langle\cos^2\theta\rangle\rangle$, $\langle\langle\cos^2\theta\rangle^2\rangle$, and $\langle\langle\cos^4\theta\rangle\rangle$ that are present in the expression for the signal for N_2 (for which both odd and even J 's are allowed).

No.	Group freq.	Weighting factor	Formula	Peak series (in Bc)	Expt. series
$\langle\langle\cos^2\theta\rangle\rangle$					
1	-	a	-	0	-
2	ω_1	b	$4J + 6$	10, 18, 26, for odd J 6, 14, 22, for even J	II I
$\langle\langle\cos^2\theta\rangle^2\rangle$					
3	-	aa'	-	0	-
4	ω_1 and ω'_1	$a'b$ and ab'	$4J + 6$	10, 18, 26, for odd J 6, 14, 22, for even J	II I
5	$\omega_1 + \omega'_1$	$\frac{bb'}{2}$	$4(J + J') + 12$	20, 28, 36, ..	III
6	$\omega_1 - \omega'_1$	$\frac{bb'}{2}$	$4(J - J') > 0$	4, 8, 12, ..	IV
$\langle\langle\cos^4\theta\rangle\rangle$					
7	-	a	-	0	-
8	ω_1	b	$4J + 6$	10, 18, 26, for odd J 6, 14, 22, for even J	II I
9	ω_2	c	$8J + 20$	28, 44, 60..	III

Table IV: All possible frequency arising from $\langle\langle\sin^2\cos^2\theta\rangle^2\rangle$ for O_2 whose only odd J 's are allowed. The weak frequencies are noticed with (*).

No.	Group freq.	Weighting factor	Formula	Peak series (in Bc)	Expt. series
1	-	aa'	-	0	-
2	ω_1 and ω'_1	$a'b$ and ab'	$4J + 6$	10, 18, 26, ...	II
3	ω_2 and ω'_2	$a'c$ and ac'	$8J + 20$	28, 44, 60, ...	III
4	$\omega_1 + \omega'_1$	$\frac{bb'}{2}$	$4(J + J') + 12$	20, 28, 36, ..	III
5	$\omega_1 - \omega'_1$	$\frac{bb'}{2}$	$4(J - J') > 0$	8, 16, 24, ..	V
6	$\omega_2 + \omega'_2$	$\frac{cc'}{2}$	$8(J + J') + 40$	56, 72, 88, ..	I*
7	$\omega_2 - \omega'_2$	$\frac{cc'}{2}$	$8(J - J') > 0$	16, 32, 48, ..	V*
8	$\omega_1 + \omega'_2$ and $\omega_2 + \omega'_1$	$\frac{bc'}{2}$ and $\frac{b'c}{2}$	$4(J + 2J') + 26$	38, 46, 54, ..	VI*
9	$\omega_1 - \omega'_2$	$\frac{bc'}{2}$	$4(J - 2J') - 14 > 0$	6, 14, 22, ...	VI*
10	$\omega_2 - \omega'_1$	$\frac{b'c}{2}$	$4(-J + 2J') + 14 > 0$	2, 10, 18, ...	II*

gives series III (**20, 28, 36, 44, ..**) Bc . All the possible series arising from these three leading terms and their grouping according to those observed experimentally are shown in table III. Note that series III is identical, and overlap, with the series IV: (**4, 8, 12, 16, ..**) Bc and adds to its strength. Moreover, the remaining lines at (**4, 8, 12, 16, 24, 32, ...**) Bc found in the experimental spectrum in Fig. 12(a) as well as in the theoretical spectrum in Fig. 12(b), confirm the existence of the series IV which is distinct from the series III. The existence of series III and IV is a prove of the fact that the dynamic signal of N_2 can not be described in term of $\langle\langle\cos^2\theta\rangle\rangle(t_d)$ only.

In Fig. 13 we compare the experimental spectrum (panel a) for O_2 [13] with the theoretical spectrum (panel b) calculated from Eq. (113). Both the experimental and the theoretical spectra in Fig. 13 show the Raman-

allowed series II: (**10, 18, 26, 34, 42, ..**) Bc , but not the series I: (6, 14, 22, 30, 38, ..) Bc , seen for N_2 . The anomalous series III: (**20, 28, 36, 44, ..**) Bc , discussed in the case of N_2 above, however, appears for O_2 as well. Finally, another anomalous sequence V: (**8, 16, 24, ..**) Bc can be seen to be present in the data for O_2 in Fig. 13a, that, we point out, can not be generated by $F.T.$ of $\langle\langle\sin^2 2\theta\rangle\rangle$ term. To interpret the origin of the observed series in O_2 we first consider the leading term given by Eq. (110), $\langle\langle\sin^2\theta\cos^2\theta\rangle^2\rangle$. The matrix element $\langle\sin^2\theta\cos^2\theta\rangle$ vanishes unless $\Delta J = 0, \pm 2, \pm 4$ corresponds to frequency ω_0, ω_1 , and ω_2 . Thus, there will be the various sum and difference frequencies that arise from the presence of the squared moment, as follows:

$$\begin{aligned}
& (a + b \cos \omega_1 t + c \cos \omega_2 t) (a' + b' \cos \omega'_1 t + c' \cos \omega'_2 t) \\
& = aa' + ab' \cos \omega'_1 t + a'b \cos \omega_1 t \\
& \quad + ac' \cos \omega'_2 t + a'c \cos \omega_2 t \\
& \quad + \frac{bb'}{2} \cos (\omega_1 + \omega'_1) t + \frac{bb'}{2} \cos (\omega_1 - \omega'_1) t \\
& \quad + \frac{cc'}{2} \cos (\omega_2 + \omega'_2) t + \frac{cc'}{2} \cos (\omega_2 - \omega'_2) t \\
& \quad + \frac{bc'}{2} \cos (\omega_1 + \omega'_2) t + \frac{bc'}{2} \cos (\omega_1 - \omega'_2) t \\
& \quad + \frac{b'c}{2} \cos (\omega_2 + \omega'_1) t + \frac{b'c}{2} \cos (\omega_2 - \omega'_1) t \quad (130)
\end{aligned}$$

with $a > b > c$. As discussed before, the frequency ω_1 generates the lines $(4J + 6)$ that for odd J give the series II: (10, 18, 26, ...) Bc . The series I: (6, 14, 22, ...) Bc that would exist for even J is absent from the O_2 spectrum. This is easily understood as due to the nuclear spin of O atoms, which is 0, that strictly forbids any even J rotational levels for O_2 (as dictated by the overall symmetry of the total wavefunction for O_2). For odd J , the frequency ω_2 produces the lines $(8J + 20)Bc = (28, 44, 60, \dots)Bc$, whereas the sum frequency $(\omega_1 + \omega'_1)$ produces the lines $(4(J + J') + 12)Bc = (20, 28, 36, \dots)Bc$; taken together they generate the series III: **(20, 28, 36, 44, ...)** Bc . Similarly, the difference frequency $\omega_1 - \omega_2$ gives rise to the series V: **(8, 16, 24, ...)** Bc , as shown in table IV. All the above predicted series are observed in the Fourier spectrum for O_2 . It is also shown in table IV that frequency $\omega_1 + \omega'_2$ and $\omega_2 + \omega'_1$ produces the weak (strength of order order "bc") series VI: $(4(J + 2J') + 26)Bc = (38, 46, 54, \dots)Bc$. Despite its weakness the existence of this series too is evidenced by the presence of the line at $38Bc$. It is worth noting that the series V and VI can not be generated from the moment $\langle \sin^2 2\theta \rangle$ alone. The remaining higher order terms in Eq. (113) contribute, generally very weakly, either to the lines in series above or to some additional lines that can be seen in Fig. 13(b), but hardly resolved in Fig. 13(a). Finally, we may point out that the heights of the few lowest frequency lines in the experimental data in Fig. 13(a) for O_2 are believed to be due to the fluctuation of the laser outputs in the experiment (see, foot-note [20] of [13]).

We may point out that during the test calculations, the relative strengths of the lines in a calculated spectrum were found to depend sensitively (cf. Fig. 14) on the assumed molecular temperature, which is rather difficult to determine experimentally. This sensitivity, on the other hand, provides a way to estimate the temperature of the molecular ensemble of interest in the experiment, by requiring that the rotational line for the maximum height of the Fourier spectrum of the dynamic signal to match with the peak of the Boltzmann distribution of the initially occupied rotational levels, and adjusting the latter to find the matching temperature.

Fig. 14 shows a calculated spectrum for initial tem-

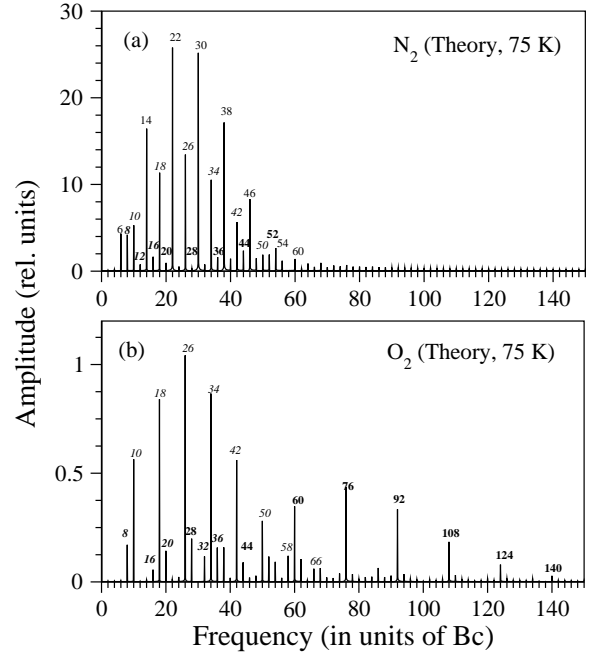


Figure 14: Calculated spectra for N_2 (panel a) and O_2 (panel b) at a Boltzmann temperature 75 K; laser parameters are as in Fig. 4 and 12, for N_2 , and, as in Fig. 5 and 13, for O_2 .

perature 75 K whose peaks are shifted from one of 200 K (Figs. 12 and 13). We also point out that our adiabatic theory produces series III in for N_2 and series V and VI for O_2 . These terms arise from the cross-term, and hence can not be produced from frozen nuclei approximation. Thus, the spectrum in frequency domain gives more succinct and clearer information of the HHG signal and therefore power full to test the model [19].

F. Interplay of Polarization Geometry α and Delay Time t_d

So far we have limited our applications to the HHG signal for parallel geometry of the pump and probe polarizations. We now consider the more general case when probe polarization is rotated by a given angle α . Fig. 15 (upper panel) shows our computational results of the HHG signals as a function of t_d , at three different fixed α , i.e. $\alpha = 0^\circ$, 45° , and 90° , for N_2 . We note that the signal for $\alpha = 90^\circ$ changes its phase by π with respect to the signal for $\alpha = 0^\circ$, a phenomenon that is also observed recently [12, 27, 55]. In contrast, the signal for $\alpha = 45^\circ$ is seen to remain rather flat with change of α .

To see qualitatively the α dependence of HHG signal of N_2 , we consider the leading term of Eq. (114) which

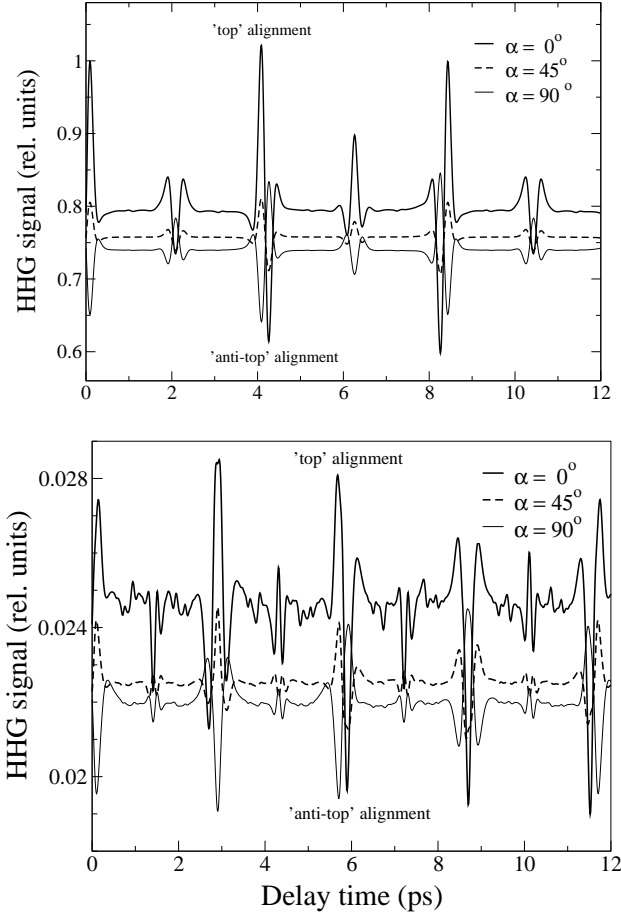


Figure 15: Calculated 19th harmonic dynamic signal for N_2 (upper panel) and O_2 (lower panel) for various pump-probe polarization angles, i.e. $\alpha = 0^\circ$, $\alpha = 45^\circ$, and $\alpha = 90^\circ$. The laser parameters are similar with one in Figs. 4 and 5 for N_2 and O_2 , respectively. The initial temperature is 200 K.

is given by

$$S^{(n)}(t_d; \alpha) = c_{00}^{(n)} + c_{01}^{(n)} \left[\frac{1}{2} \sin^2 \alpha + \frac{1}{2} (3 \cos^2 \alpha - 1) \times \langle \langle \cos^2 \theta \rangle \rangle (t_d) \right] + \dots \quad (131)$$

Thus, for the parallel polarizations we have, $S^{(n)}(t_d; 0^\circ) \approx c_{00}^{(n)} + c_{01}^{(n)} \langle \langle \cos^2 \theta \rangle \rangle (t_d)$ and for the perpendicular polarizations, $S^{(n)}(t_d; 90^\circ) \approx c_{00}^{(n)} + \frac{c_{01}^{(n)}}{2} (1 - \langle \langle \cos^2 \theta \rangle \rangle (t_d))$ which are clearly of opposite phase as a function of t_d . These above expressions also show that the modulation depth for $\alpha = 90^\circ$ is smaller than one for $\alpha = 0^\circ$, that can not be obtained by planar model [12]. Eq. (131) also implies that the extrema of the signal would occur for $\sin \alpha \cos \alpha = 0$, or the maximum at $\alpha = 0^\circ$ and the minimum for $\alpha = 90^\circ$, as seen in Fig. 15(upper) and confirmed experimentally [12, 26, 55]. Eq. (131) also implies that at a critical angle α_c given by $(3 \cos^2 \alpha_c - 1) = 0$, or $\alpha_c \approx 55^\circ$, the

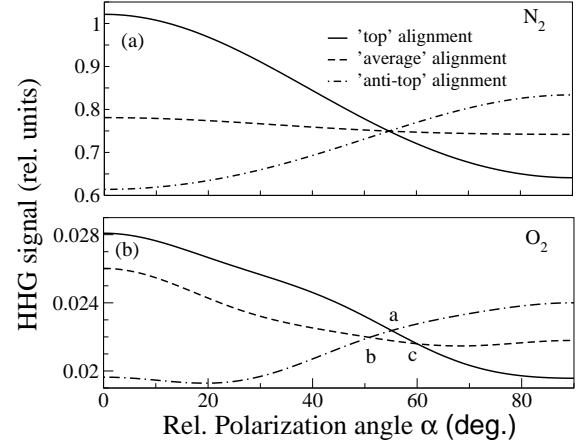


Figure 16: Variation of the 19th HHG signal as a function of pump-probe polarization angle α , near the first half-revival, for N_2 (upper panel). The observation times are $t_d = 4.090$ ps for the “top”, $t_d = 4.180$ ps, the “average”, and $t_d = 4.265$ ps the “anti-top” alignment times. And similarly for O_2 (lower panel). The pulse parameters are the same as in Fig. 4 for N_2 and Fig. 5 for O_2 . The initial temperature is 200 K. Note the existence of a “magic” angle at $\alpha = \arctan \sqrt{2} \approx 55^\circ$ for N_2 , where the dynamical signals all coincide, and a “crossing neighborhood” near that angle for O_2 .

signal essentially remains constant and *independent* of the delay t_d between the pulses. This geometry therefore can be used to generate a steady state HHG signal from N_2 , with femtosecond pulses.

The magic angle in fact is a generic signature for the σ_g symmetry of the active molecular orbitals.

For O_2 , the leading term of HHG signal (Eq. (115)) reads

$$S^{(n)}(t_d; \alpha) = \frac{c_{11}^{(n)}}{64} \langle ((-35 \cos^4 \alpha + 30 \cos^2 \alpha - 3) \times \langle \cos^4 \theta \rangle (t_d) + (30 \cos^4 \alpha - 24 \cos^2 \alpha + 2) \langle \cos^2 \theta \rangle + (-3 \sin^4 \alpha + 4 \sin^2 \alpha))^2 \rangle + \dots \quad (132)$$

Thus, for the parallel polarizations we have, $S^{(n)}(t_d; 0^\circ) \approx c_{11}^{(n)} \langle (-\langle \cos^4 \theta \rangle + \langle \cos^2 \theta \rangle)^2 \rangle = c_{11}^{(n)} \langle \langle \sin^2 \theta \cos^2 \theta \rangle^2 \rangle$ and for the perpendicular polarizations, $S(t_d; 90^\circ) \approx \frac{c_{11}^{(n)}}{64} \langle (-3 \langle \cos^4 \theta \rangle + 2 \langle \cos^2 \theta \rangle + 1)^2 \rangle$. It was clear that the sign of $\langle \cos^4 \theta \rangle$ does not change and hence the phase of eighth revival also remains constant, as shown in Fig. 15 (lower panel) and confirmed experimentally [12, 27, 55]. These above expressions also can be expressed as $S(t_d; 90^\circ) \approx c_{11}^{(n)} \langle (\frac{3}{8} \langle \sin^2 \theta \cos^2 \theta \rangle - \frac{1}{8} \langle \cos^2 \theta \rangle + \frac{1}{8})^2 \rangle$ shows that the modulation depth for $\alpha = 90^\circ$ is smaller than one for $\alpha = 0^\circ$, that can not be obtained by planar

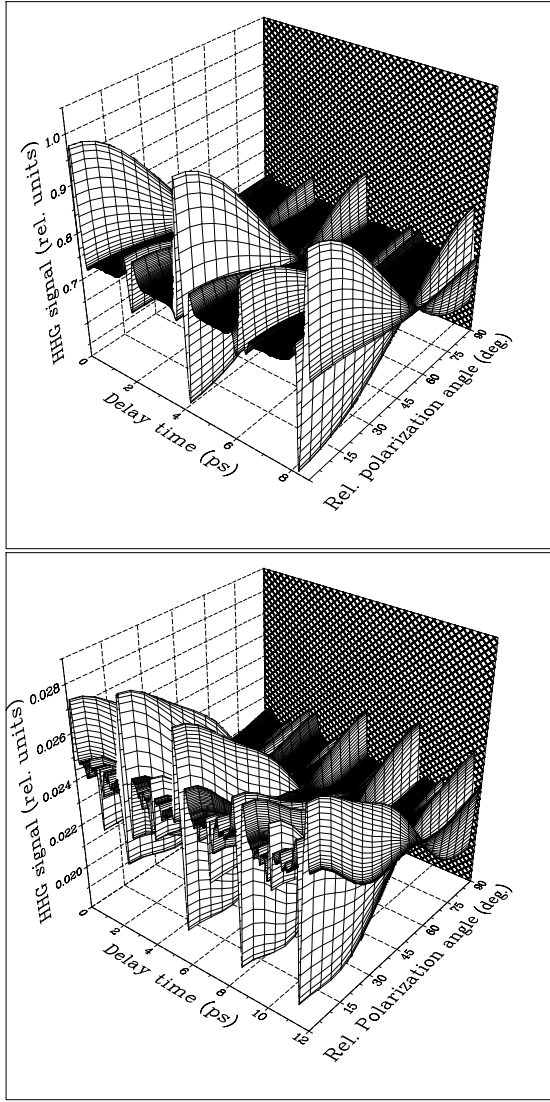


Figure 17: HHG signals for N₂ (upper panel) and O₂ (lower panel) as simultaneous function of delay time t_d and the relative angle α between the pump and probe polarizations. The laser parameters are similar to that in 4 and 5 for N₂ and O₂, respectively. The initial temperature is 200 K.

model [12].

We also calculated the signal at fixed time delay for various relative polarization direction between pump and probe pulses. In Fig. 16 we show the results for N₂ (upper panel) and for O₂ (lower panel), near the first revival $t_d \approx \frac{1}{2}T_{rev}$. For the case of N₂ a coincidence of the signals is seen to occur at a critical angle $\alpha_c \approx 55^\circ$. This is fully consistent with the prediction of the near t_d -independence of the signal for N₂ at α_c , made above. The HHG signal (solid curve) at $t_d = 4.090$ ps (‘top’-alignment) lies above the signal at $t_d = 4.265$ ps (‘anti-top’ alignment), for all angles α smaller than the critical $\alpha_c \approx 55^\circ$; the opposite relation holds above α_c . For the case of O₂ (lower panel), in contrast, there is no single critical value of α where the signals for all t_d ’s could co-

incide. This is due mainly to the different α -dependence of $\langle \cos^2 \theta \rangle$ and $\langle \cos^4 \theta \rangle$ of Eq. (120). Nevertheless, it can be seen that the signal at the ‘top’ alignment becomes equal to the signal at the ‘anti-top’ alignment not far from $\alpha_c \approx 55^\circ$ (Point a, Fig. 16(b)), and they reverse their relative strengths above it. During the calculation, we get that the exact position of points *a*, *b*, and *c* depend on the initial temperature. These whole properties well agree with the experimental data [26, 55]. We also note that the calculated α -dependent signal given by Zhou *et al.* gives the same properties for N₂, but they predicted the signal for O₂ to be maximized at $\alpha \approx 45^\circ$.

In Fig. 17, we plot the calculated signals as function of both the delay time t_d and relative polarization angles α for both N₂ (upper panel) and N₂ (lower panel). For both molecules, the modulation depths decrease by increasing relative polarization angle, reach zero near critical angle $\alpha_c \approx 55^\circ$, and increase again but in opposite phase above the critical angle. The results for $\theta = 90^\circ - 180^\circ$ are exactly mirror image of the results for $\theta = 0^\circ - 90^\circ$.

Before concluding this section it is also worthwhile to point out that the α -dependence of the HHG signals for the more complex tri-atomic molecule CO₂ and the organic molecule acetylene, $HC \equiv CH$, because of their active π orbital symmetry, are predicted from the general structure of the HHG signal given by Eq. (103) (even with out detailed calculations) to exhibit a “cross-over” neighborhood near $\alpha \approx 55^\circ$; this is indeed the case, as has been recently observed experimentally [63]. Clearly, the presence of the “magic” angle and the cross-over neighborhood provide a signature of the symmetry of the active molecular orbital, which can be useful in the context of the “inverse” problem of molecular imaging [64] from the HHG data as suggested first in [20]. Finally, the agreement between the present results and experimental data provides a clear possibility to control the HHG signals by varying both the time- delay *and* the relative pump-probe polarization angle, simultaneously.

VII. SOME PROBLEMS OF GENERAL INTEREST RELATED TO PUMP-PROBE SIGNALS FOR HHG

Before concluding this paper we report on the results of our investigations of a number of pump-probe experiment related problems of interest in the present context.

A. Effect of Probe Pulse on the Alignment

In pump-probe experiments it is generally assumed that the dynamical alignment of the molecular axis is governed by the ultrashort pump pulse, while the ultrashort probe pulse that leads to the HHG signal does not affect the alignment. To check the validity or otherwise of this assumption, we directly compare here the dynamic alignment moment, $A(t_d; \alpha = 0)$ calculated as usual as-

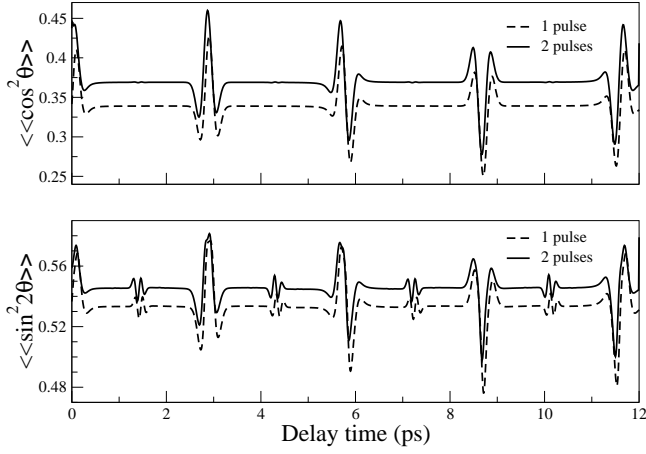


Figure 18: Shift of the alignment signal vs. delay time: $\langle\langle\cos^2\theta\rangle\rangle$ for N₂ (upper panel), and $\langle\langle\sin^2 2\theta\rangle\rangle$ for O₂ (lower panel) at 300 K; $I_{\text{pump}} = 0.8 \times 10^{14} \text{ W/cm}^2$ and $I_{\text{probe}} = 1.7 \times 10^{14} \text{ W/cm}^2$ with FWHM 40 fs. See, text for further explanation.

suming when only the pump and when both pump and probe pulse couple to the molecular polarizability, for N₂. In the latter case, the total field consists of the superposition of the two pulses with a displacement Δt in time between them:

$$\begin{aligned} \mathbf{F}(t) &= \mathbf{F}_1 \cos(\omega_1 t) + \mathbf{F}_2 \cos(\omega_2(t - \Delta t)) \\ &= \varepsilon_{10} \sqrt{g_1(t)} \cos(\omega_1 t) \\ &\quad + \varepsilon_{20} \sqrt{g_2(t - \Delta t)} \cos(\omega_2(t - \Delta t)) \end{aligned} \quad (133)$$

and

$$\begin{aligned} \langle\varepsilon^2(t)\rangle &= \frac{1}{2}\varepsilon_{10}^2 g_1(t) + \frac{1}{2}\varepsilon_{10}^2 g_1(t - \Delta t) \\ &\quad + 2\varepsilon_{10}\varepsilon_{20} g_1(t) g_2(t - \Delta t) \\ &\quad \times \langle(\cos(\omega_1 t))(\cos(\omega_2(t - \Delta t)))\rangle \end{aligned} \quad (134)$$

In the above the indices 1 and 2 stand for pump and probe pulse, respectively. Suppose the data are recorded after the probe pulse dies out, then the observing time is $t = \Delta t + \tau$, where τ is the duration of the probe pulse. Eq. (134) then reads

$$\begin{aligned} \langle\varepsilon^2(\Delta t + \tau)\rangle &= \frac{1}{2}\varepsilon_{10}^2 g_1(\Delta t + \tau) + \frac{1}{2}\varepsilon_{10}^2 g_1(\tau) \\ &\quad + 2\varepsilon_{10}\varepsilon_{20} g_1(\Delta t + \tau) g_2(\tau) \\ &\quad \times \langle(\cos(\omega_1(\Delta t + \tau)))(\cos(\omega_2\tau))\rangle \end{aligned} \quad (135)$$

showing its dependence on the delay between the two pulses Δt and the length of interaction of the probe pulse τ . In Fig. 18, we plot the alignment moment $\langle\langle\cos^2\theta\rangle\rangle(\Delta t + \tau)$ and $\langle\langle\sin^2 2\theta\rangle\rangle(\Delta t + \tau)$ for O₂, plotted as a function of delay between two pulses Δt , for a fixed $\tau = 40$ fs, as shown by the solid curve. The results

are compared with that obtained from the pump pulse alone (dashed curve), recorded at the same time. The comparison clearly shows that the probe pulse changes the dynamic alignment $\langle\langle\cos^2\theta\rangle\rangle(t_d)$ in that the signal is shifted upward by the presence of the probe pulse as may be expected from the enhanced intensity of the field when both the pulses overlap significantly (before it dies out). Thus, except perhaps when the two pulses overlap (or are separated only negligibly) this does *not* change the general characteristics of the dynamical signals. Therefore, within the above mentioned exception, one may neglect the effect of the probe pulse on the HHG signal.

B. Effect of Initial Temperature

We assume that the rotational eigenstates $|J_0 M_0\rangle$ of the molecule are occupied thermally before the interaction with the pump pulse. Unlike an upward transition $(J_0, M_0) \rightarrow (J'_0, M_0)$ to the states with an arbitrarily high J'_0 , the downward transition toward $J'_0 \geq M_0$ can be restricted. As a result, a wavepacket state created by the pump pulse would consist of eigenstates with higher occupation of $J'_0 \geq M_0$, implying that the vector of rotational angular momentum would tend to lie in a plane perpendicular to the pump polarization direction. Since the rotational angular momentum itself is perpendicular to the internuclear axis of a linear molecule, the above condition, $J'_0 \geq M_0$, means also that the molecular axis would tend to align in the direction of the laser polarization. This is the physical reason why the alignment angle of the molecular axis with respect to the polarization direction after the laser interaction is generally smaller after the interaction than before it, i.e. the degree of alignment increases on interaction with the pump pulse. Since at a lower initial temperature, the lower M_0 states are relatively more occupied initially, the “degree of alignment” $A \equiv \langle\langle\cos^2\theta\rangle\rangle$ would tend to be higher, allowing the molecules to be more readily aligned at a lower initial temperature.

C. Mean Energy of the Molecule after the Pump Pulse

It is interesting also to examine the way the mean energy of the molecule changes with increasing intensity of the pump pulse. Fig. 20 shows the calculated mean energy $\langle E \rangle_{J_0 M_0}(t)$ at a time t , before and after the arrival of the peak of the pump pulse (of length t_p). As expected, the figure shows that increasing the peak pulse intensity, increases the mean energy of the molecule or, the “effective temperature” $T_{\text{eff}} \equiv \langle E \rangle_{J_0 M_0}(t > t_p) / k_B$, where k_B is the Boltzmann constant. However, it should be remembered that after the pulse interaction, the molecular system is not a state of thermal equilibrium, rather it is in a state of dynamical equilibrium (or steady state) that can not be characterized thermodynamically.

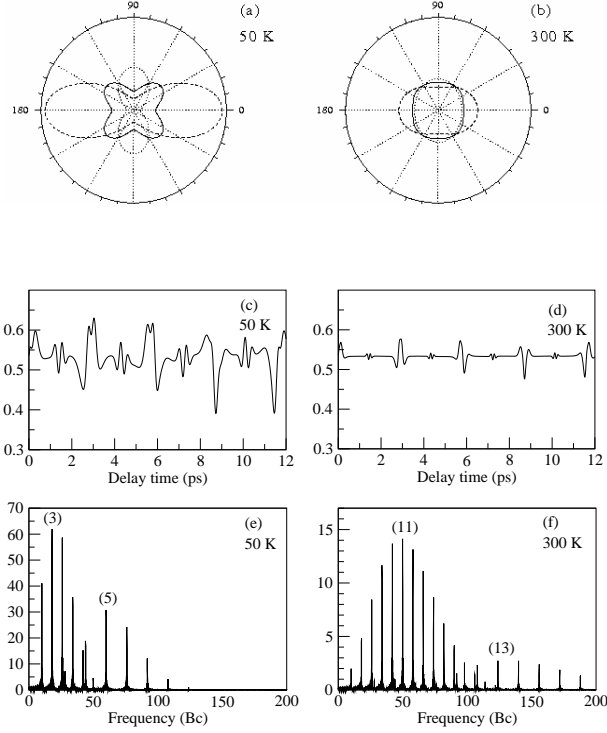


Figure 19: Influence of the initial temperature, 50° or 300° , on the molecular axis-distribution (panel a-b), on the leading dynamic moment $\langle \sin^2 2\theta \rangle(t_d)$ (panel c-d), and the Fourier spectrum (panel e-f) of the latter, for the case of O_2 . The molecular axis-distribution (panel a-b) are given at three values of the delay time t_d , i.e. at the “top” alignment $t_d = 5.649$ ps (dashed line), at the “average” alignment $t_d = 5.812$ ps (solid line), and at the “anti-top” alignment $t_d = 5.975$ ps (dotted line); the radii are in the same scale. $I = 0.5 \times 10^{14}$ W/cm² and FWHM=40 fs.

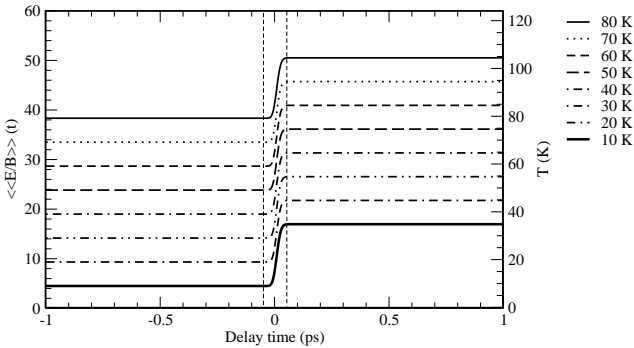


Figure 20: Mean energy of O_2 before and after interaction with the laser pulse, for different initial temperatures. The vertical dashed lines indicate the extent of the pulse duration; $I = 0.5 \times 10^{14}$ W/cm² FWHM=40 fs. See, text for further explanation.

To estimate an effective “temperature” of the rotational wavepacket states $|\Phi_{J_0 M_0}(t)\rangle$, in the steady state regime, i.e. for $(t_{pump} \leq t \leq t_{probe})$, we note (a) that the rotational wavepacket states $|\Phi_{J_0 M_0}(t)\rangle$ form a linearly independent set of states like the set of rotational eigenstates $|J_0 M_0\rangle$ from which they evolve, (b) that the individual rotational wavepacket states evolve in *one-to-one* correspondence with the initially occupied rotational eigenstates $|J_0 M_0\rangle$, (c) that the mean energy of each of the rotational wavepacket states reach a steady state, also one-to-one of energy from $\langle E \rangle_{J_0 M_0}(t > t_{pump}) = E_{J_0 M_0} + \langle E \rangle_{J_0 M_0}(t \geq t_{pump})$. If further the above change in the mean energy $\langle E \rangle_{J_0 M_0}(t > t_{pump}) - \langle E \rangle_{J_0 M_0}(t \geq t_{pump})$ is *independent* of the the individual states chosen (indices $\{J_0 M_0\}$) then one might use it to define an effective “temperature” change, ΔT_{eff} , given by

$$\Delta T_{eff} = \frac{\langle \Delta E \rangle(t \geq t_{pump})}{k_B} \quad (136)$$

We may note in Fig. 20, that the change in the mean energy in the steady state regime is indeed essentially independent of the states of the system chosen. Thus, the effective “temperature” of the system, at the end of the interaction with the pump pulse, becomes

$$T_{eff} = T_0 + \Delta T_{eff} \quad (137)$$

Note that T_{eff} is in general greater than the initial gas (jet) temperature, T_0 , and it tends to increase with the increase of the pump intensity. Later on we shall describe a method of determining this “effective temperature” of the system from a theoretical analysis of the experimental HHG data.

D. Some Non-equivalent Definitions of the HHG Signal

In this sub-section we briefly discuss two alternative definitions of HHG signals that have been employed earlier and compare them with the definition of the HHG signal of the present theory, and with experimental data. The present theory defines the quantum transition amplitudes for the linearly independent reference states $|\chi_i(t)\rangle, i \equiv \{e, J_0 M_0\}$, (consisting of the product of the ground electronic and the coherent rotational wavepacket states) to obtain the independent harmonic emission probabilities, and in accordance with the quantum statistical theory averages the latter to define the HHG signal (cf. e.g. Eq.(62):

$$S^{(n)}(t_d) = \mathcal{C} \sum_{J_0 M_0} \rho(J_0) \left| \left\langle \Phi_{J_0 M_0}(t_d, \theta) \left| T_e^{(n)}(\theta) \right| \Phi_{J_0 M_0}(t_d, \theta) \right\rangle \right|^2 \quad (138)$$

It is worth noting that the quantum amplitude calculation in the present theory corresponds to the “adiabatic

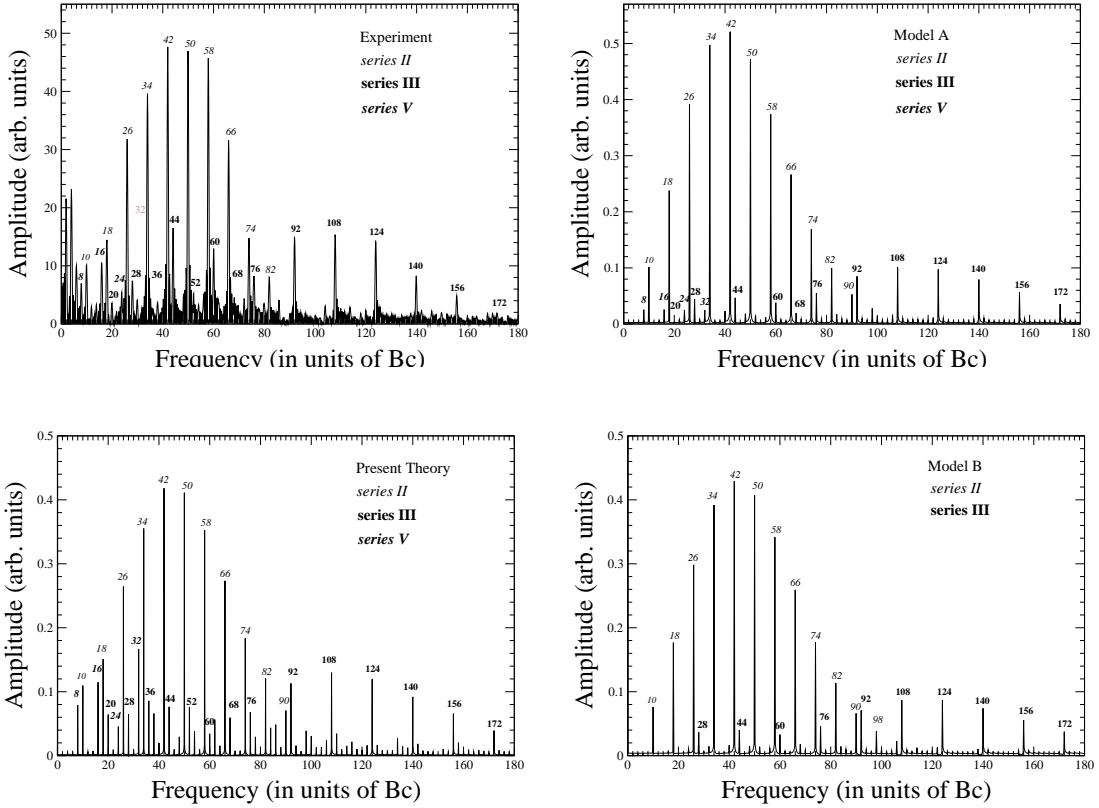


Figure 21: Theoretical Fourier spectrum of the dynamic 19th harmonic signal for O_2 ; pump intensity $I = 0.5 \times 10^{14} \text{ W/cm}^2$, probe intensity $I = 1.2 \times 10^{14} \text{ W/cm}^2$, duration 40 fs, wavelength 800 nm, and temperature 200 K. The calculations are done using the present theory, Eq. (138), (left-lower panel), model A Eq.(139), (right-upper panel), and model B, Eq. (140), (right-lower panel). For comparison, the experimental spectrum (left-upper panel) is also shown.

nuclei” approximation [61, 62], in which the matrix elements with respect to the rotational wavepacket states are evaluated at the level of the adiabatic amplitude-operator, $T^{(n)}(\theta)$, and *not* at the level of the adiabatic probability-operator, $|T^{(n)}(\theta)|^2$, that occurs in the more drastic “frozen nuclei” approximation. In this theory, as in the laboratory, the operational angle is the relative polarization angle α , and *not* the angle between the polarization direction and the molecular axis, θ . In fact, the angle θ is a coordinate that is, as appropriate for a quantum formulation, to be *integrated over* to obtain the quantum transition amplitude with respect to the rotational wavepacket states.

In the present notation, the two other definitions of the HHG signal that have been used earlier (to be referred to below as A and B) are, (i) definition A (cf. Eq. (22) of [25] and Eq. (6) of [65]):

$$S_A^{(n)}(t_d) = \mathcal{C} \left| \sum_{J_0 M_0} \rho(J_0) \langle \Phi_{J_0 M_0}(t_d, \theta) | T_e^{(n)}(\theta) | \Phi_{J_0 M_0}(t_d, \theta) \rangle \right|^2$$

and, (ii) definition B (cf. Eq. (12) of [24] and Eq. (4) of

[66]):

$$S_B^{(n)}(t_d) = \mathcal{C} \sum_{J_0 M_0} \rho(J_0) \left\langle \Phi_{J_0 M_0}(t_d, \theta) \left| T_e^{(n)}(\theta, 0) \right|^2 \Phi_{J_0 M_0}(t_d, \theta) \right\rangle$$

Clearly the HHG signals according to models A and B differ with each other, and they differ from the present definition, Eq. (138) above.

We note that model A, Eq. (139), defines the statistically averaged signal by weighting the individual amplitudes (!) first, and then taking the absolute square of the weighted sum. This runs counter to the quantum statistical theoretical approach of averaging the probabilities (not amplitudes) and/or the expectation values of Hermitian observables themselves, and not their Fourier transforms (that are proportional to the emission amplitudes). Furthermore, the definition of model A (Eq. (139)) makes the signal to depend on the mixed products of the statistical weights that are in principle *independent*.

The signal defined by model B, Eq. (140), is seen to depend on the weighted sum of the diagonal matrix elements (between the rotational wavepacket states) of the “probability operator” $|T^{(n)}(\theta)|^2$ – this, of course, is

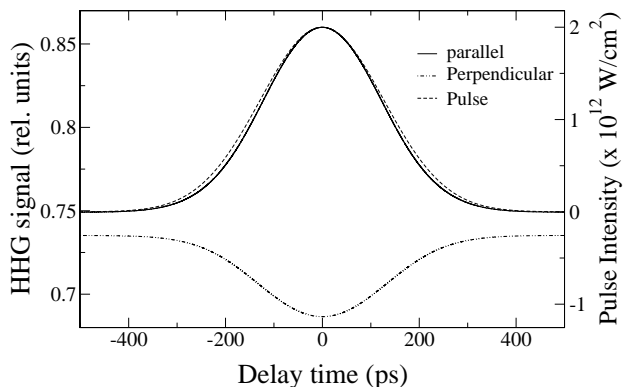


Figure 22: Calculated 9th HHG spectrum of N_2 for various pump-probe polarizations angle $\alpha = 0^\circ$ and $\alpha = 90^\circ$; pump intensity $I = 2 \times 10^{12} \text{ W/cm}^2$, duration 300 ps; probe intensity, $I = 5 \times 10^{14} \text{ W/cm}^2$, duration 70 fs, and wavelength 798 nm; Boltzmann temperature 25 K.

not equal to the weighted sum of the absolute squares of the diagonal matrix elements of the transition operator $T^{(n)}(\theta)$. In model B the above circumstance is a consequence of the more drastic “frozen nuclei” approximation and an effective inclusion of *all* transitions, those between the same wavepacket states (“elastic-like”) *as well as* those between the different wavepacket states (“inelastic-like”). However, unlike in model A (Eq. (139)), in model B (Eq. (140)) the weighted statistical sum is taken, in accordance with the quantum statistical theory, at the level of the probabilities.

In Fig. 21 we show a comparison of the experimental data (upper-left panel) of the *F.T.* of the dynamic signal ($\alpha = 0$) of the 19th harmonic, for the case of O_2 with the results of the test calculations from: the present theory (lower-left panel) using Eq. (138), model A (upper-right panel) using Eq. (139), and model B (lower-right panel) using Eq. (140), keeping everything else the same – the parameters are the same as in Fig. 13. The similarity of the calculated spectrum from the present theory and the experimental data is seen to be very satisfactory, that from model A is similar, except that the ratio of the peaks of the series III to series II is generally too small compared to the experimental data, and series V (**8, 16, 24, ..**) *Bc* is rather weakly developed. In the case of model B, on the other hand, the series V (**8, 16, 24, ..**) *Bc* is simply missing. It may be noted that the present comparison also illustrates the ability of the experimental data at the level of the (discrete) Fourier spectrum, to better distinguish between the various theoretical models than may be possible at the level of the time-domain signal.

E. Adiabatic Alignment

Finally, we apply the present dynamic theory also to the adiabatic case, in which we choose a long (300 ps)

pump pulse and a short (70 fs) probe pulse, as in an adiabatic alignment experiment [67] used earlier. The results of our calculations for N_2 , using Eqs. (114) for both $\alpha = 0^\circ$ (solid curve), and $\alpha = 90^\circ$ (dash-dot curve), are shown in Fig. 22. For the sake of comparison we also show the intensity profile (dashed curve) of the pump pulse (right scale). As can be seen immediately from the figure, in the parallel case, the HHG signal closely follows the evolution of the long pump pulse itself (which might be expected for an adiabatic process) and the maximum of the signal occurs at the maximum of pulse, for $\alpha = 0^\circ$. On the other hand, a minimum is predicted for the signal at the maximum intensity, in the perpendicular case, for $\alpha = 90^\circ$. These characteristics of the adiabatic signals for N_2 are consistent with the experimental observations made some time ago [67, 68, 69].

VIII. CONCLUSIONS

To conclude, we have presented an *ab initio* intense-field S-matrix theory of dynamic alignment of linear molecules and the characteristic HHG signals from them as detected in intense-field femtosecond pump-probe experiments. Useful analytical expressions for the molecular alignment and the HHG signal as a function of both the delay-time, t_d , and the relative polarization angle, α , between the pump and probe pulse, are derived. Thus, we give the general HHG signal Eq. (103), the signal for N_2 (generically, active σ_g orbital symmetry) Eq. (114), or its leading term Eq. (131), as well as the signal for O_2 (generically, active π_g orbital symmetry) Eq. (115), or its leading term, Eq. (132). They are used to make detailed analysis of the molecular alignment and the observed experimental data for the HHG signals from coherently rotating N_2 and O_2 molecules, both in the time-domain *and* in the frequency domain. The results show a remarkable agreement between the theory and the experimental observations. Additional predictions about the existence of critical relative polarization angles, α_c , and their relation to the symmetry of the active orbitals and the form of the dynamic signals are made. At a “magic” angle, $\alpha_c \approx 55^\circ$, the dynamic HHG signals for all delay times t_d , are predicted to approach each other closely for a linear molecule with a σ_g orbital symmetry, or exhibit a “crossing neighborhood”, for the π_g orbital symmetry; it is also predicted to produce a steady emission of high harmonic radiation at the magic angle from N_2 . Moreover, we have investigated a number of theoretical questions and experimental effects of general interest in connection with the interpretation of the pump-probe HHG signals. Finally, we have shown that the case of “adiabatic-alignment”, and the resulting HHG signal, can be analyzed and understood equally well within the present dynamical theory, using simply a long duration of the pump pulse.

Acknowledgments

We thank Prof. K. Miyazaki for providing the experimental data in digital form shown in the upper panels of

Figs. 4, 5, 12, 13, and 21, and for useful discussions.

-
- [1] J.H. Posthumus, Rep. Prog. Phys. **67**, 623 (2004).
 - [2] A. Becker and F.H.M. Faisal, J. Phys. B **38**, R1 (2005).
 - [3] T. Seideman, Phys. Rev. Lett. **83**, 4971 (1999).
 - [4] J. Ortigoso, M. Rodriguez, M. Gupta, and B. Friedrich, J. Chem. Phys. **110**, 3870 (1999).
 - [5] L. Cai, J. Marango and B. Friedrich, Phys. Rev. Lett. **86**, 775 (2001).
 - [6] H. Stapelfeldt and T. Seideman, Rev. Mod. Phys. **75**, 543 (2003).
 - [7] I.V. Litvinyuk, K.F. Lee, P.W. Dooley, D.M. Rayner, D.M. Villeneuve, and P.B. Corkum, Phys. Rev. Lett. **90**, 233003 (2003).
 - [8] P.W. Dooley, I.V. Litvinyuk, K.F. Lee, D.M. Rayner, M. Spanner, D.M. Villeneuve, and P.B. Corkum, Phys. Rev. A **68**, 023406 (2003).
 - [9] M. Kaku, K. Masuda, and K. Miyazaki, Japan. J. Appl. Phys. **43**, 591, (2004).
 - [10] D. Zeidler, J. Levesque, J. Itatani, K. Lee, P. W. Dooley, I. Litvinyuk, D.M. Villeneuve, and P.B. Corkum in *Ultrafast Optics IV*, ed. F. Krausz *et. al.* (Springer, New York, 2004) p. 247.
 - [11] J. Itatani, D. Zeidler, J. Levesque, M. Spanner, D.M. Villeneuve and P.B. Corkum, Phys. Rev. Lett. **94**, 123902 (2005).
 - [12] T. Kanai, S. Minemoto and H. Sakai, Nature **435**, 03577 (2005).
 - [13] K. Miyazaki, M. Kaku, G. Miyaji, A. Abdurrouf, and F.H.M. Faisal, Phys. Rev. Lett. **95**, 243903 (2005).
 - [14] J. Itatani, J. Levesque, D. Zeidler, H. Niikura, H. Pepin, J.C. Kieffer, P.B. Corkum and D.M. Villeneuve, Nature **432**, 867 (2004).
 - [15] J. Levesque, J. Itatani, D. Zeidler, H. Pepin, J.C. Kieffer, P.B. Corkum, and D.M. Villeneuve, J. Mod. Opt. **53**, 185 (2006).
 - [16] S. Patchkovskii, Z. Zhao, T. Brabec, and D.M. Villeneuve, Phys. Rev. Lett. **97**, 123003 (2006).
 - [17] S. Baker, J.S. Robinson, C.A. Haworth, H. Teng, R.A. Smith, C.C. Chirila, M. Lein, J.W.G. Tisch, and J.P. Marangos, Science **312**, 424 (2006).
 - [18] N.L. Wagner, A. Wuest, I.P. Christov, T. Popmintchev, X. Zhao, M.M. Murnane, and H.C. Kapteyn, PNAS, **103**, 13279 (2006).
 - [19] F.H.M. Faisal, A. Abdurrouf, K. Miyazaki, and G. Miyaji, Phys. Rev. Lett. **98**, 143001 (2007).
 - [20] F.H.M. Faisal, and A. Abdurrouf, Phys. Rev. Lett. **100**, 123005 (2008).
 - [21] F. Rosca-Pruna and M.J.J. Vrakking, J. Chem. Phys. **116**, 6575 (2002).
 - [22] G. Herzberg, *Molecular Spectra and Molecular Structure, I* (Van Nostard Reinhold, New York (1950), chap. III.
 - [23] X.X. Zhou, X.M. Tong, Z.X. Zhao and C.D. Lin, Phys. Rev. A **71**, 061801(R) (2005).
 - [24] X.X. Zhou, X.M. Tong, Z.X. Zhao and C.D. Lin, Phys. Rev. A **72**, 033412 (2005).
 - [25] C.B. Madsen and L.B. Madsen, Phys. Rev. A **74**, 023403 (2006).
 - [26] M. Kaku, R. Morichi, G. Miyaji, and K. Miyazaki, IEEE on Quantum Electronics Conference 2005, paper QWG4-3, p. 1036.
 - [27] K. Yoshii, G. Miyaji, K. Miyazaki, A. Abdurrouf, and F.H.M. Faisal, IEEE on CLEO - Pacific Rim 2007, p. 660 (2007).
 - [28] R.P. Feynman, *Quantum Electrodynamics* (Benjamin Inc., New York, 1962).
 - [29] J.J. Sakurai, *Modern Quantum Mechanics* (Addison-Wesley, New York, 1994).
 - [30] L.V. Keldish, Zh. Eksp. Teor. Fiz. **47**, 1945 (1964) [Sov. Phys. JETP **20**, 1307 (1964)].
 - [31] F.H.M. Faisal, J. Phys. B **6**, L89 (1973).
 - [32] H.R. Reiss, Phys. Rev A **22**, 1786 (1980).
 - [33] J.D. Jackson, *Classical Electrodynamics* (J. Wiley & Sons, New York, 1962).
 - [34] W.H. Press, B.P. Flannery, S.A. Teukolsky, and W.T. Vetterling, *Numerical Recipes: The Art of Scientific Computing* (Cambridge University Press, 1986).
 - [35] We may assume as usual that the field envelopes are slowly varying compared e.g. to the periods of the higher harmonics.
 - [36] P. Salières, B. Carré, L. Le Déroff, F. Grasbon, G. G. Paulus, H. Walther, R. Kopold, W. Becker, D. B. Milošević, A. Sanpera, and M. Lewenstein, Science **4292**, 902 (2001).
 - [37] We may note that the above holds strictly for an ideal medium with a constant velocity of propagation. In dispersive media the frequency and the wavenumbers are related by the frequency dependent velocity of propagation $v = c/n(\Omega)$ where n is the frequency dependent refractive index of the medium. This necessitates a much more detailed analysis of the phase-matching condition, that has been carried out (see e.g. [36]) by solving the associated Maxwell's equations for the propagating fields, numerically in specific cases. The results indicate rather generally an effective phase matching, for the higher harmonics. In the presence of ionization, the medium becomes also dissipative. In a weakly ionized medium the effect may be taken into account by including a decay factor $e^{-\frac{1}{2}\gamma_i(t+t')}$ that is to be multiplied with the expression of the integrand of the HHG amplitude (or of the dipole expectation value), where γ_i is the total rate of ionization of the reference bound state $i \equiv |\chi_i(t)\rangle$.
 - [38] M. Ferray, F. Gounand, P. D'Oliveira, P. R. Fournier, D. Cubaynes, J. M. Bizau, T. J. Morgan, and F. J. Wuilleumier, Phys. Rev. Lett. **59**, 2040 (1987).
 - [39] A. McPherson, G. Gibson, H. Jara, U. Johann, T.S. Luk, I.A. McIntyre, K. Boyer, and C.K. Rodes, J. Opt. Soc. Am. B **4**, 595 (1987).
 - [40] F. Ehlötzky, Phys. Rep. **345**, 175 (2001).
 - [41] T. Seideman, J. Chem. Phys. **115**, 5965 (2001).
 - [42] M. Lewenstein, Ph. Balcou, M. Yu. Ivanov, A. L'Huillier and P.B. Corkum, Phys. Rev. A **49**, 2117 (1994).

- [43] F.E. Harris and H.H. Michels, J. Chem. Phys. **43**, S165 (1965).
- [44] F.H.M. Faisal, J. Phys. B **3**, 636 (1970).
- [45] D. A. Varshalovich, A.M. Moskalev and V.K. Khersonskii, *Quantum Theory of Angular Momentum* (Word Scientific, Singapore, 1988).
- [46] R. N. Zare, *Angular Momentum: Understanding Spatial Aspects in Chemistry and Physics* (Wiley, New York, 1988).
- [47] I.S. Gradshteyn and I.M. Rhysik, *Table of Integral, Series, and Product* (Academic Press, New York, 1965).
- [48] X.M. Tong, Z.X. Zhao, and C.D. Lin, Phys. Rev. A **66**, 033402 (2002).
- [49] T.K. Kjeldsen, and L.B. Madsen, Phys. Rev. A **71**, 023411 (2005).
- [50] W.L. Jorgensen and L. Salem, *The Organic Chemist's Book of Orbital* (Academic Press, New York, 1973)
- [51] A.M. James and M.P. Lord, *MacMillan's Chemical Physical Data* (MacMillan, London, 1992).
- [52] J.O. Hirschfelder, C.F. Curtis, and R.B. Bird, *Molecular Theory of Gases and Liquids* (Wiley, New York, 1954).
- [53] S. Ramakrishna and T. Seideman, Phys. Rev. Lett. **99**, 113901 (2007).
- [54] S. Ramakrishna and T. Seideman, Phys. Rev. A **77**, 053411 (2008).
- [55] K. Miyazaki (personal communication).
- [56] F. Rosca-Pruna and M.J.J. Vrakking, J. Chem Phys. **116**, 6567 (2002).
- [57] I. Sh. Averbukh and N.F. Parelman, Phys. Lett. A **139**, 449 (1989).
- [58] M.J.J. Vrakking, D.M. Villeneuve, and A. Stolow, Phys. Rev. A **54**, R37 (1996).
- [59] R. Bluhm, V.A. Kosteletsky, and J.A. Porter, Am. J. Phys. **64**, 994 (1996).
- [60] S. Fleischer, I. Sh. Averbukh, and Y. Prior, Phys. Rev. A **74**, 041403(R) (2006).
- [61] D.M. Chase, Phys. Rev. **104**, 835 (1956).
- [62] F.H.M. Faisal and A. Temkin, Phys. Rev. Lett. **28**, 203 (1972).
- [63] R. Torres, N. Kajumba, J. G. Underwood, J. S. Robinson, S. Baker, J. W. G. Tisch, R. de Nalda, W. A. Bryan, R. Velotta, C. Altucci, I. C. E. Turcu, and J. P. Marangos, Phys. Rev. Lett. **98**, 203007 (2007).
- [64] M. Lein, J. Phys. B **40**, R135 (2007).
- [65] C. B. Madsen, A. S. Mouritzen, T. K. Kjeldsen, and L. B. Madsen, Phys. Rev. A **76**, 035401 (2007).
- [66] A.T. Le, X.-M. Tong, and C. D. Lin Phys. Rev. A **73**, 041402(R) (2006).
- [67] R. Velotta, N. Hay, M.B. Mason, M. Castillejo, and J.P. Marangos, Phys. Rev. Lett., **87**, 183901 (2001).
- [68] N. Hay, R. Velotta, M.Lein, R. de Nalda, E. Hessel, M. Castillejo, and J.P. Marangos, Phys. Rev. A **65**, 053805 (2002).
- [69] N. Hay, M.Lein, R. Velotta, R. deNalda, E. Hessel, M. Castillejo, P.L. Knight, and J.P. Marangos, J. Mod. Opt. **50**, 561 (2003).